https://doi.org/10.5194/egusphere-2026-2127
Preprint. Discussion started: 22 April 2026

Impact of high-resolution soil erodibility datasets on dust simulations in WRF-Chem with the GOCART scheme

Leandro C. Segado-Moreno[1], Juan Pedro Montávez[1], Ginés Garnés-Morales[2], Eloisa Raluy-López[1], Pedro Jiménez-Guerrero[1,3], and Rajesh Kumar[4]

[1]Physics of the Earth, Regional Campus of International Excellence (CEIR) "Campus Mare Nostrum", University of Murcia, Murcia, Spain
[2]Department of Meteorology, University of Reading, Reading, United Kingdom
[3]Biomedical Research Institute of Murcia (IMIB-Arrixaca), Murcia, Spain
[4]National Center for Atmospheric Research (NCAR), Boulder, United States

Correspondence: Leandro C. Segado-Moreno (leandrocristian.segadom@um.es)

Abstract.

Mineral dust is a major atmospheric aerosol influencing climate, air quality, and human health through radiative and microphysical processes. The Iberian Peninsula is frequently affected by North African dust intrusions, leading to episodic PM_{10} exceedances that challenge air quality forecasting. However, accurate representation of dust emissions remains limited by uncertainties in soil erodibility, land surface properties, and meteorological forcing.

This study evaluates the impact of two high-resolution soil erodibility datasets on dust simulations using WRF-Chem with the GOCART scheme. The first dataset, EROD-HR, integrates fine-resolution topography to improve dust source representation at 0.0625° (∼5 km) globally and 1 km over the Iberian Peninsula. The second dataset, SOILHD, further refines dust source characterization by incorporating high-resolution soil texture (sand, silt, and clay fractions) and removing misclassified bare-soil areas, resulting in a 1 km global resolution. Both datasets aim to better capture the spatial heterogeneity of dust sources.

Simulations are conducted for five dust episodes between 2022 and 2025, covering local and long-range transport conditions. Model performance is evaluated against PM_{10} observations from the SINQLAIR network in the Region of Murcia. Results show improved representation of dust emissions, with better agreement in magnitude and timing of PM_{10} peaks at inland stations. Improvements are more limited at coastal and anthropogenically influenced sites, although statistical metrics (correlation, bias, RMSE) indicate consistent gains.

Overall, high-resolution erodibility datasets enhance dust simulations by reducing biases and improving variability representation, highlighting the importance of detailed land-surface information for regional dust forecasting systems.

1 Introduction

Mineral dust is one of the most abundant atmospheric aerosols and exerts a significant influence on the Earth's radiation budget through radiative and microphysical processes (Masson-Delmotte et al., 2021). Dust particles scatter and absorb solar and terrestrial radiation, affecting surface and atmospheric heating rates through aerosol direct and semidirect effects (Johnson

https://doi.org/10.5194/egusphere-2026-2127
Preprint. Discussion started: 22 April 2026

et al., 2004; Chung, 2012). In addition, mineral aerosols act as cloud condensation and ice-nucleating particles, modifying cloud microphysics, lifetime, and precipitation processes (Tegen and Schepanski, 2009; Kok et al., 2018). These interactions may also influence large-scale atmospheric circulation patterns (Garnés-Morales et al., 2023). Furthermore, dust episodes significantly affect air quality, visibility, and human health at regional and local scales (Mahowald et al., 2007; Tong et al., 2023; Garnés-Morales et al., 2025), as fine particles can penetrate deep into the respiratory system, increasing the risk of respiratory and cardiovascular diseases and premature mortality (Schraufnagel, 2020; Tarín-Carrasco et al., 2021).

The Iberian Peninsula (IP) is frequently affected by dust intrusions originating from North Africa (NA), particularly during spring and summer (Querol et al., 2009; Pey et al., 2013; Salvador et al., 2022; López-Cayuela et al., 2025). These intrusions contribute significantly to surface concentrations of particulate matter with an effective diameter of 10 μm or less (PM_{10}) and 2.5 μm or less ($PM_{2.5}$), often exceeding European air quality standards (Beloconi and Vounatsou, 2023). In this context, chemistry transport models (CTMs), coupled both online and offline with numerical weather prediction (NWP) models, arise as a key tool to understand and forecast extreme dust concentration events. Accurate simulation of dust events is essential to support mitigation strategies, public health warnings, and operational air quality forecasting systems, as well as better meteorological forecasts. However, simulating dust emission and transport remains a major challenge due to uncertainties in the representation of dust sources, land surface characteristics, and meteorological drivers, particularly at the regional scale (Knippertz and Todd, 2012; Jin et al., 2020; Kok et al., 2020; Rahmati et al., 2020; Zhao et al., 2020, 2021; Ratcliffe et al., 2024; Tan et al., 2025).

Among the CTMs, the Weather Research and Forecasting model coupled with Chemistry (WRF-Chem) has been widely employed for the simulation of mineral dust emissions and transport at regional scales (Grell et al., 2005). WRF-Chem has become a widely used tool for investigating dust emissions and transport due to its ability to interactively simulate meteorological and chemical processes (Rizza et al., 2017; Palacios-Peña et al., 2019; Zeng et al., 2020; Zhao et al., 2020; Lee et al., 2024). One of the most commonly used aerosol schemes among the multiple available within WRF-Chem is the Goddard Chemistry Aerosol Radiation and Transport (GOCART) scheme (Ginoux et al., 2001). The balance between computational efficiency and accuracy in dust representation makes GOCART suitable for both research and operational applications using WRF-Chem (e.g., Palacios-Peña et al., 2020; Jerez et al., 2021; Georgiou et al., 2022; Pino-Carmona et al., 2024; Yarragunta et al., 2025, among many others). The GOCART scheme considers five species of aerosols: black carbon, organic carbon, dust (5 size-distributed bins), sea salt (5 bins), and sulfates. For the estimation of dust emissions, the GOCART scheme employs surface wind speed, soil moisture, vegetation cover, and a soil erodibility factor that determines the susceptibility of the surface to wind-driven dust uplift (Ginoux et al., 2001; LeGrand et al., 2019). Despite the widespread use of the GOCART scheme, the default EROD dataset in WRF-Chem is based on a coarse-resolution (0.25°) global topography dataset, which limits its capacity to capture small-scale variations in surface conditions, vegetation cover, and topography that critically affect dust emission processes. This limitation is particularly problematic in regions like the southern IP, where semi-arid conditions, heterogeneous land surface properties, sparse vegetation, and varying soil moisture lead to localized high-emission dust sources that are inadequately represented in coarse-resolution datasets. As a result, dust emissions and surface concentrations are often underestimated in these regions, leading to discrepancies between model simulations and observations. Incorporating a

https://doi.org/10.5194/egusphere-2026-2127
Preprint. Discussion started: 22 April 2026

high-resolution topographic dataset can enhance the spatial characterization of dust source areas, providing a more realistic representation of surface conditions for dust emission parameterizations.

Some previous studies attempted to create a more realistic erodibility field in the past, based on ground measurements, satellite products, or both. For example, Li et al. (2023) created a dataset in which erodibility is computed as a function of soil texture, vegetation coverage, soil moisture, and land use, using satellite products (e.g., NDVI, soil moisture) to dynamically modulate the potential for wind erosion. Their study focused on the East Asia region, dominated by the presence of the Gobi and Taklimakan Deserts, which promote high-concentration dust events periodically. However, when looking at the Sahara Desert, the erodibility dataset retrieves unrealistically high values across the entire region, promoting excessively high concentrations. Additionally, the dataset provides moderate erodibility values over high mountain areas with permanent snow or ice, such as the Alps, which are clearly unrealistic. In a recent study, Lee et al. (2025) proposed a similar method that integrates both satellite-derived land-cover characteristics and surface dust observations over the same region. However, their main goal was to determine the capability of the dataset to characterize dust source regions, not to assess the quality of the new dataset with NWP simulations. Spyrou et al. (2022) developed a dynamic dust source map for the GOCART/AFWA mechanism in the WRF-Chem model by incorporating vegetation variability derived from MODIS NDVI data to vary seasonally in response to changes in surface vegetation cover. Two simulations were carried out for the spring of 2017 over the Mediterranean and the Middle East, one using the default dust source map and another using the NDVI-based scheme. The simulations were compared against AERONET aerosol optical depth (AOD) observations. Results showed that the NDVI-based simulation substantially improved model performance, particularly during intense dust events (AOD $>$ 0.25), reducing bias and root mean square error (RMSE), while increasing correlation with observations (Spyrou et al., 2022). Although the proposed approach shows promising results, the study does not include a direct comparison between the NDVI-based dust source map and other existing erodibility databases, relying instead on separate case studies for each configuration.

In this study, the development and application of two new high-resolution global erodibility datasets are presented. Firstly, a high-resolution, topography-based dataset, named EROD-HR, was created (Segado-Moreno et al., 2026a). EROD-HR incorporates the fine-resolution GMTED2010 elevation dataset (Danielson and Gesch, 2011), which is also employed in WRF as the default elevation dataset, and is crafted following the methodology described by LeGrand et al. (2019) as a first approach to enhance the representation of dust sources in WRF-Chem simulations using the GOCART scheme. Secondly, to further improve the representation of local-scale dust uptake sources while accounting for the heterogeneity of soil composition (and therefore the dust size distribution), which varies greatly both locally and globally, a novel, local-scale, soil-type-dependent dataset named SOILHD was created (Segado-Moreno et al., 2026b). This dataset aims to extend and refine the new high-resolution EROD-HR field by explicitly incorporating spatial variations in soil composition while removing areas erroneously identified as bare soil by previous datasets. Specifically, the relative mass fractions of sand, silt, and clay at each grid cell were computed. To accomplish this, we have employed the 0-5 cm layer of the soil type fraction dataset ISRIC SoilGrids at a 250 m resolution (Hengl et al., 2017; Poggio et al., 2021), together with bare soil estimates, sourced from a global map of Local Climate Zones developed by Demuzere et al. (2022) and available open source in Demuzere et al. (2023). The new EROD-HR dataset achieves a spatial resolution of 0.0625° (≈5 km) globally and 1 km locally for the IP, a region frequently affected by

https://doi.org/10.5194/egusphere-2026-2127
Preprint. Discussion started: 22 April 2026

dust events as a consequence of its proximity to the Sahara Desert and the presence of highly erodible soils and semi-arid climate conditions. Meanwhile, the SOILHD dataset achieves a 1 km resolution globally.

To evaluate the impact of the new high-resolution datasets, an ensemble of case studies is run, including some above-average PM_{10} concentration events from both local and convective transport sources. The simulations are validated against ground-based PM_{10} measurements from the regional SINQLAIR network in the Region of Murcia (RM), allowing for the assessment of improvements in the spatial and temporal representation of dust concentrations. Statistical metrics, such as correlation coefficients, mean bias error (MBE), and root mean square error (RMSE), were computed to quantify model performance. This work aims to evaluate the benefits of employing a high-resolution soil erodibility dataset in operational dust forecasting systems for southern Europe, while also contributing to the advancement of high-resolution modeling by demonstrating the added value of incorporating detailed topography into the soil erodibility parameterizations used in regional air quality models.

2 Data and methods

2.1 The GOCART scheme and the new erodibility database

In the GOCART scheme, for a given size bin p, the dust emission flux value (kg m^{-2} s^{-1}) is obtained for each surface model cell using the following equation (Ginoux et al., 2001; LeGrand et al., 2019):

$$F_p = C\,S\,s_p\,U^2\,(U - U_t(D_p,\theta_s))\,, \qquad U > U_t(D_p,\theta_s) \tag{1}$$

where C is a dimensional proportionality constant, S is a unitless dust source strength function, s_p is the mass fraction of emittable dust from a given dust bin at the surface, U is the horizontal wind speed at 10 m, and U_t is the threshold 10-meter wind speed required to initiate erosion for a given particle diameter D_p and soil surface wetness θ_s. F_p is 0 in any other case where U does not exceed the threshold velocity. Once U_t is surpassed, the dust source function S arises as the key parameter to determine the location and amount of dust emitted. S was originally computed by Ginoux et al. (2001) based on the idea that dust material is often generated in alluvial processes and accumulates in low points. For this reason, S was determined based on the degree of topographic relief surrounding a model grid cell using the following equation (LeGrand et al., 2019):

$$S = \left(\frac{z_{max} - z_i}{z_{max} - z_{min}}\right)^5 \tag{2}$$

where z_i is the elevation of the cell, and z_{max} and z_{min} are the maximum and minimum elevation in a $10^\circ \times 10^\circ$ window centered on the same grid cell. S is set to 0 anywhere bare soil is not indicated by the Advanced Very High Resolution Radiometer (AVHRR) data (DeFries et al., 1999). At the time of this study, the GOCART scheme in WRF uses a precalculated source strength function S, stored in the code as the variable EROD, which is read in and interpolated to the model grid by the WRF-Chem preprocessor (LeGrand et al., 2019). This static field was calculated by applying Eq. 2 to a 0.25° resolution elevation dataset. This results in a coarse-resolution dust source dataset, which limits its ability to represent local-scale dust sources accurately (Figs. 3 and 6).

https://doi.org/10.5194/egusphere-2026-2127
Preprint. Discussion started: 22 April 2026

2.2 Creation of the new databases

In a first step to overcome the spatial limitations of the default 0.25° erodibility field, a new high-resolution dataset (hereafter EROD-HR) was developed following the original formulation of the dust source strength function (Eq. 2), while incorporating higher-resolution and more physically consistent geophysical inputs. The main objective was to improve the spatial representativeness of potential dust sources, particularly in regions where local terrain variability, land cover, and soil texture exert a dominant control on dust uplift. The dust source strength function S was recalculated globally using the GMTED2010 elevation model (Danielson and Gesch, 2011). The native 7.5-arcsecond (≈250 m) topographic data were resampled to a 0.0625° (≈5 km) spatial resolution to balance physical detail and computational feasibility for regional WRF-Chem applications. For the inner domains covering the IP and the RM, a 1 km version was generated to enable fine-scale validation and to assess the impact of convective-scale topographic variability on dust emission.

To ensure physical consistency with the GOCART emission formulation, only grid cells identified as barren or sparsely vegetated were considered active dust sources. Land cover classification was derived from the MODIS 20-category global land use dataset (Friedl et al., 2002), and non-erodible classes (e.g., urban areas, forests, croplands, permanent water bodies, and snow or ice) were masked by setting S=0. This ensures that dust uplift is restricted to areas where bare-soil exposure is physically plausible. The resulting dataset preserves the conceptual structure of the original erodibility field while substantially improving its spatial fidelity.

In WRF-Chem, soil texture is represented in a simplified manner within the dust emission formulation. The erodibility field is defined by three layers corresponding to the soil textural classes contributing to dust emission: sand, silt, and clay. In the standard scheme (Ginoux et al., 2001), constant global mass fractions are assumed for all grid cells (50% sand, 25% silt, and 25% clay). Accordingly, the EROD-HR dataset was constructed by multiplying the recalculated S field by these fixed fractions. As a result, EROD-HR remains fully compatible with the internal WRF-Chem structure while incorporating higher-resolution topographic and land-cover information. This 50-25-25% sand-silt-clay assumption has also been adopted in other recent erodibility datasets based on satellite-derived indicators of soil erosion and vegetation scarcity (Li and Wang, 2022; Spyrou et al., 2022). Nevertheless, assuming uniform soil composition can lead to unrealistic dust emission strengths in regions with pronounced soil heterogeneity. To address this limitation, an enhanced erodibility dataset, termed SOILHD (Soil-Type Heterogeneous Dataset), was developed by replacing the fixed soil fractions with spatially variable, observation-based soil composition fields (Fig. 1).

https://doi.org/10.5194/egusphere-2026-2127
Preprint. Discussion started: 22 April 2026

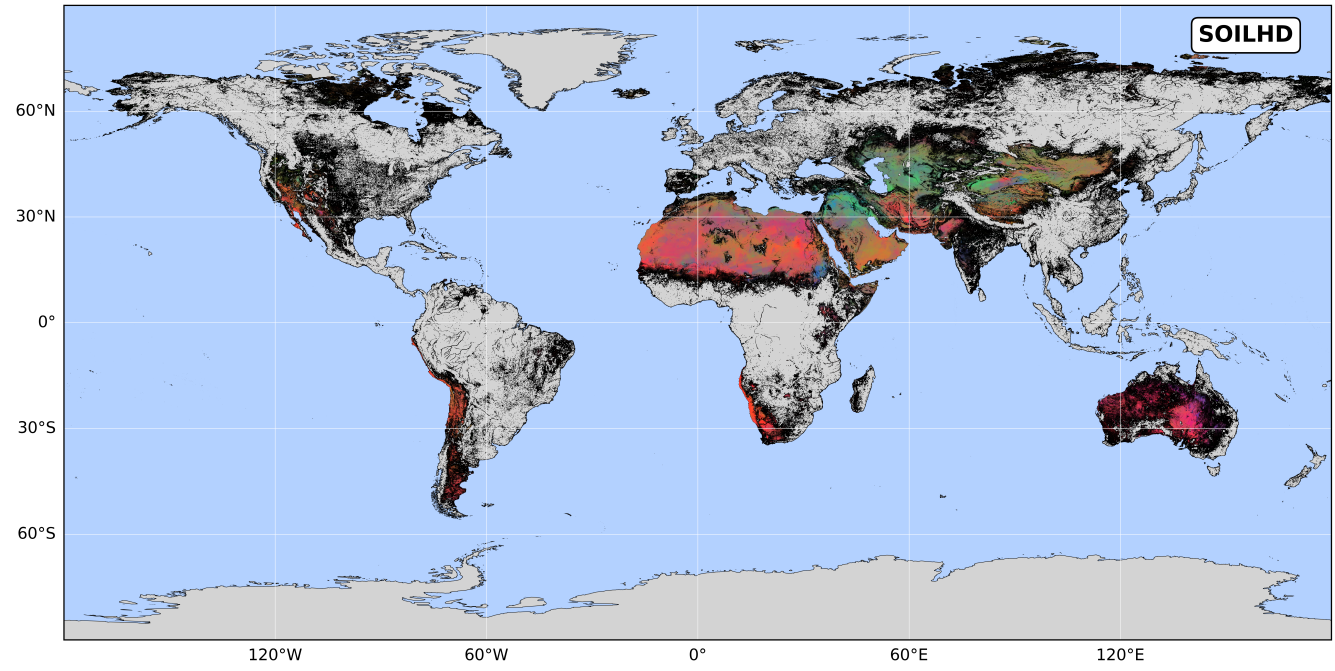

Figure 1. Three-band (RGB) representation of the SOILHD dataset. Each soil type layer (sand, silt, and clay) is depicted by a color band (red, green, and blue, respectively). The color intensity reflects the overall erodibility value. Grey color means no erodible soil available.

SOILHD data were derived from two complementary sources. First, the ISRIC SoilGrids250m database (Hengl et al., 2017; Poggio et al., 2021), which provides global predictions of soil properties (including sand, silt, and clay fractions) based on machine-learning models trained on more than 230,000 soil profile observations at 250 m spatial resolution and multiple depth layers (0–200 cm), was employed. Only the 0-5 cm layer was used in this study. The effective radii associated with the silt and clay fractions correspond to the GOCART dust size bins: bin 1 for clay (0-1 μm) and bins 2 -4 for silt (1- 10 μm).

Secondly, the global map of Local Climate Zones (LCZs) developed by Demuzere et al. (2022) was used to identify potential dust source areas while excluding surfaces erroneously classified as bare soil in previous datasets, such as high-mountain regions, urban areas, snow- and ice-covered surfaces, and greenhouses. This dataset consists of a global LCZ map at 100 m spatial resolution, derived from multiple Earth observation products and LCZ class labels (Demuzere et al., 2023). The LCZ typology (Stewart and Oke, 2012) distinguishes urban and natural surface types based on characteristic combinations of land cover and physical properties. Of the 17 LCZ classes, 10 correspond to built environments, while the remaining seven represent natural land-cover classes. For the purposes of this study, the natural barren-soil class was extracted and aggregated to a 1 km resolution grid, yielding a global map of barren-soil fraction for each grid cell.

For each soil texture class c (sand, silt, clay), a spatially explicit mass fraction field $f_c(x, y)$ was computed by averaging the 0–5 cm layer and converted into binary format. The erodibility layer for the soil class c for the SOILHD dataset (E_c) was then

https://doi.org/10.5194/egusphere-2026-2127
Preprint. Discussion started: 22 April 2026

defined as:

$$E_c(x,y) = f_c(x,y) \cdot B(x,y) \tag{3}$$

where $B(x,y)$ denotes the barren-soil fraction at each grid point. For the SOILHD dataset, E_c is equivalent to the source strength function S in Eq. 1. This formulation introduces realistic spatial variability in soil composition while restricting dust emission to locations where surface conditions are suitable for dust uplift at a 1 km scale. The resulting dataset provides three distinct erodibility layers per grid cell with physically based weighting factors that reflect local soil texture, rather than relying on globally uniform constants. This refinement enhances the ability of WRF-Chem to represent regional heterogeneities in dust emission intensity, particularly across transitions between sand-dominated and fine-grained soils.

Both the EROD-HR and SOILHD datasets were reprojected onto a regular latitude-longitude grid, converted to binary format, and stored following the same three-dimensional structure as the default erodibility file to ensure direct compatibility with the WRF Preprocessing System (WPS).

Finally, the new datasets were validated against the original erodibility field to ensure structural continuity (see Sect. 3.1), and the SOILHD dataset was rescaled to match the order of magnitude of the default erodibility values (see Sec. 2.3). Test simulations confirmed that both datasets were correctly ingested and interpolated by WRF-Chem without requiring any modifications to the dust emission code. The EROD-HR dataset serves as a baseline high-resolution product emphasizing improved topographic and land-cover representation, whereas SOILHD further incorporates soil-texture heterogeneity to refine the physical characterization of dust source potential.

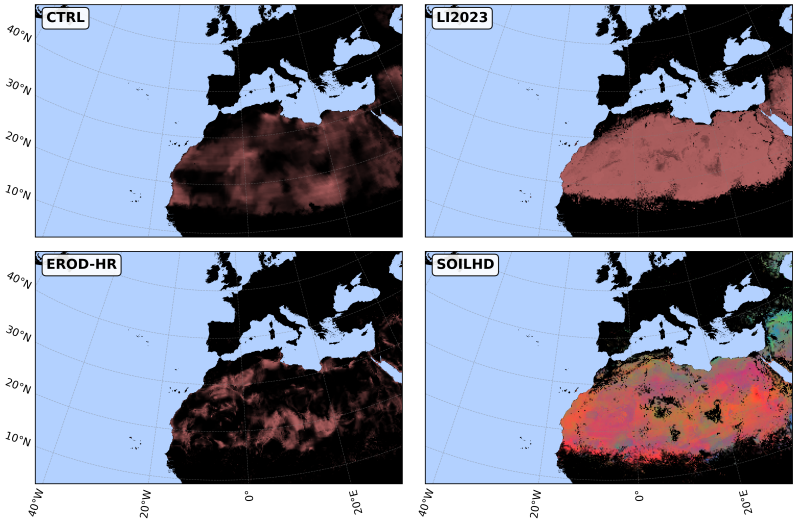

Figure 2. Soil erodibility fields (sand layer) of the 4 experiments (CTRL, LI2023, EROD-HR, and SOILHD) for domain d01.

https://doi.org/10.5194/egusphere-2026-2127
Preprint. Discussion started: 22 April 2026

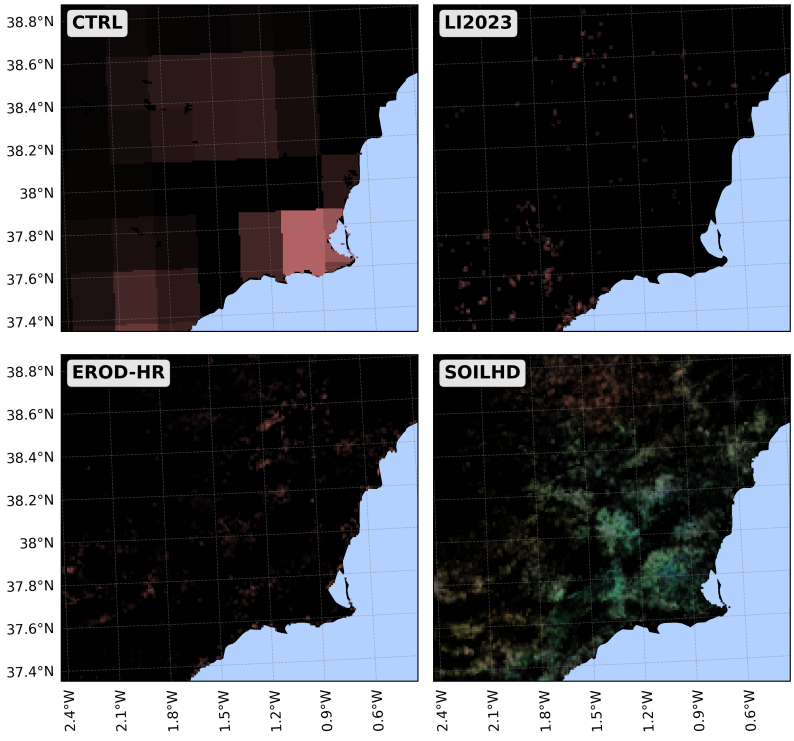

Figure 3. As Fig. 2, but for domain d03.

2.3 Tuning the erodibility database: the *EROD Tuner* tool

The tuning of soil erodibility is a common practice in dust modeling, particularly when introducing new erodibility datasets or transferring models across regions with contrasting soil, land-use, and climatic characteristics. Previous studies (e.g. Darmenova et al. (2009); Eltahan et al. (2018); Parajuli et al. (2019); Ukhov et al. (2020); Li et al. (2023)) have shown that moderate, physically motivated adjustments to erodibility can substantially improve the representation of dust emissions and downwind concentrations.

To allow a simple, systematic tuning of the erodibility field, we developed the *EROD Tuner* tool (Segado-Moreno and Montavez, 2026). This utility operates directly on the *EROD* variable contained in the WPS geo_em.d0n.nc files, modifying the soil erodibility prior to the WRF-Chem integration. Working at the preprocessing stage ensures that the modified erodibility is consistently propagated through the entire modeling workflow, while allowing different tuning strategies to be applied independently to each model domain.

A key feature of *EROD Tuner* is its flexibility. The tool supports a wide range of conversion functions, from simple linear scaling to nonlinear formulations targeting specific portions of the erodibility distribution. These include polynomial functions that damp extreme values, power-law transformations that enhance weakly erodible soils, logarithmic and sigmoid functions introducing saturation effects, and hybrid formulations that smoothly combine linear and nonlinear behavior. This flexibility

https://doi.org/10.5194/egusphere-2026-2127
Preprint. Discussion started: 22 April 2026

allows the erodibility response to be tailored to different physical hypotheses, such as increased soil cohesion, threshold-like transitions between erodible and non-erodible surfaces, or the suppression of unrealistically strong source areas.

All conversion functions are formulated in a generic, dimensionless form, making them applicable to erodibility datasets beyond those presented here. A dedicated namelist allows the selection of different functions and parameters for each nested domain, enabling region-specific tuning while preserving a unified modeling framework. This design facilitates sensitivity analyses, uncertainty assessments, and intercomparison studies in which the impact of erodibility assumptions must be isolated. The code also allows straightforward implementation of additional custom functions. The *EROD Tuner* tool is fully open-source and is publicly available on Zenodo (https://zenodo.org/records/18606994).

In the present study, the tuning applied to the SOILHD erodibility dataset was intentionally conservative. The adjustment was limited to a uniform linear scaling of the total erodibility, defined as the sum of the sand, silt, and clay components. A constant multiplicative factor of 10^{-1} was applied to bring SOILHD erodibility values into the same order of magnitude as the default WRF erodibility field. This approach preserves the spatial variability and relative contrasts introduced by SOILHD while ensuring comparability with the standard model configuration.

2.4 WRF-Chem model data

Both the initial and boundary meteorological conditions (IC and BC, respectively) used in this study were obtained from the European Centre for Medium-Range Weather Forecasts (ECMWF) fifth-generation reanalysis dataset (ERA5), which provides global coverage at a horizontal resolution of 0.25° and an hourly temporal resolution (Hersbach et al., 2018).

2.5 Observational data

Modeled dust concentrations (PM_{10}) were evaluated against ground-based observations within the innermost model domain (d03) using data from the Regional Air Quality Monitoring Network of the RM (SINQLAIR) (Regional SINQLAIR air quality network). SINQLAIR is operated by the regional government and provides high-quality, real-time measurements of major atmospheric pollutants for regulatory assessment and public information, with a native temporal resolution of 10 minutes.

The network currently consists of 11 fixed monitoring stations distributed across urban, industrial, and rural environments, as well as one mobile unit deployed during specific campaigns or pollution episodes. SINQLAIR routinely measures concentrations of particulate matter (PM_{10} and $PM_{2.5}$), nitrogen oxides (NO_x, NO_2), sulfur dioxide (SO_2), tropospheric ozone (O_3), carbon monoxide (CO), and other trace pollutants.

Based on data availability for the simulated periods, 8 stations were selected for the present analysis. These stations are listed in Table 1, and their geographical locations are shown in Fig. A1. To ensure temporal consistency with the model output, the observational time series were aggregated to hourly mean values.

https://doi.org/10.5194/egusphere-2026-2127
Preprint. Discussion started: 22 April 2026

Table 1. List of PM_{10} observational stations from SINQLAIR network used for domain 3 analysis.

No	Station	Longitude	Latitude	Name
1	ALC	-1.2321	37.9745	Alcantarilla
2	CAR	-1.8687	38.1147	Caravaca
3	ALU	-0.9144	37.6020	Alumbres
4	ALJ	-1.0659	37.6925	Aljorra
5	MOM	-0.9762	37.6018	Monpean
6	LOR	-1.7028	37.6878	Lorca
7	ESC	-0.9265	37.5744	Escombreras
8	SBA	-1.1459	37.9923	San Basilio

2.6 Model Configuration and Experiment design

The Weather Research and Forecasting model coupled with Chemistry (WRF-Chem v4.6.0) was employed to simulate a set of dust events over the RM using the Goddard Chemistry Aerosol Radiation and Transport (GOCART) aerosol scheme, which explicitly represents the emission, transport, deposition, and removal of dust particles (Ginoux et al., 2001; Grell et al., 2005).

The model configuration consists one domain with horizontal resolutions of 9 km (d01), 5 km (d02), and 1 km (d03), covering North Africa and southern Europe, the IP and the RM, respectively (Fig. 4). The model employs 30 vertical levels extending up to 10 hPa, with enhanced resolution near the surface to better resolve boundary layer processes critical for dust emission and transport.

The physical parameterization includes the Morrison two-moment microphysics scheme, the Grell–3D cumulus parameterization (applied to domains d01 and d02 only, as convection is explicitly resolved in the 1 km domain), the RRTMG shortwave and longwave radiation schemes, the Yonsei University (YSU) planetary boundary layer scheme, and the Noah land surface model. A complete list of model options and references is provided in Table 2.

The chemical mechanism selected was the simplified GOCART scheme without ozone chemistry (WRF option 300). ERA5 reanalysis data were used to provide initial and boundary meteorological conditions for the outer domain (d01).

The performance of the newly developed erodibility datasets was evaluated over several simulation periods (Table 3). Among them, the 2025–08 period corresponds to a summer dust event characterized by a persistent high-pressure system over the IP with weak pressure gradients, favoring high temperatures and elevated PM concentrations driven by both local dust uplift and convective transport. Under these conditions, the physical configuration of the erodibility field plays a particularly critical role.

For this reason, a substantial part of the results discussed in this study focuses on the 2025-08 simulations, although all periods are analyzed and discussed throughout the manuscript. For each simulation, the first day was discarded as spin-up to ensure model stability and is therefore excluded from the results analysis.

https://doi.org/10.5194/egusphere-2026-2127
Preprint. Discussion started: 22 April 2026

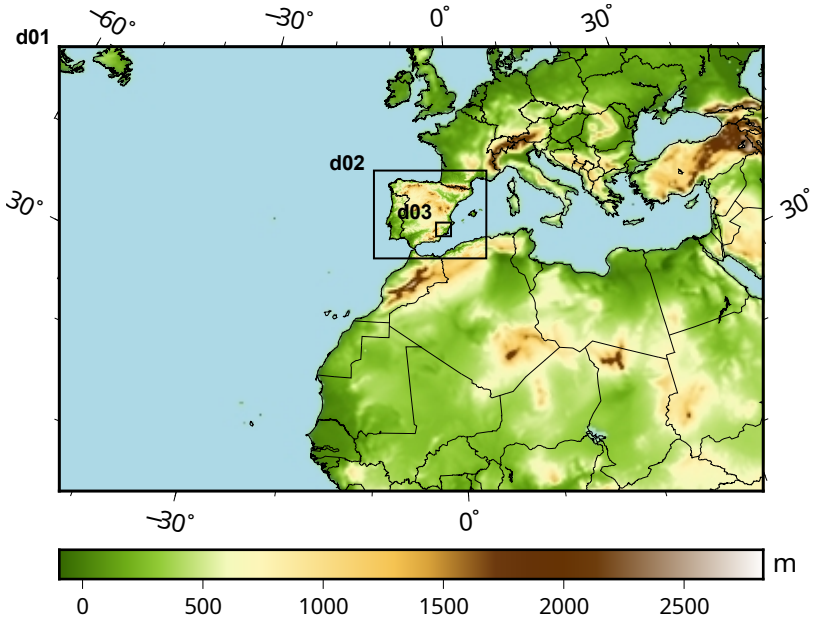

Figure 4. Domain of WRF model simulations. The nested domains d02 and d03 are shown in a black frame.

Table 2. WRF 4.6.0 configuration used in the model simulations.

Process	Option	Namelist option	Reference
Microphysics	Morrison 2-moment	mp_physics = 10	Morrison et al. (2005)
Shortwave radiation	RRTMG	ra_sw_physics = 4	Iacono et al. (2008)
Longwave radiation	RRTMG	ra_lw_physics = 4	Iacono et al. (2008)
Cumulus parametrization	Grell-3D	cu_physics = 5	Grell (1993); Grell and Dévényi (2002)
Boundary layer	YSU scheme	bl_pbl_physics = 1	Hong et al. (2006)
Land surface model	Unified Noah	sf_surface_physics = 2	Chen and Dudhia (2001)
Surface layer	Revised MM5	sf_sfclay_physics = 1	Jiménez et al. (2012)
Chemistry and aerosols	GOCART simple	chem_opt = 300	Ginoux et al. (2001)

For each period, three experiments were conducted. The first, denoted as the control (CTRL) simulation, employed the default WRF-Chem erodibility dataset. The second, referred to as EROD-HR, utilized the newly developed high-resolution EROD dataset. Finally, the SOILHD experiment incorporated the further enhanced Soil-Type Heterogeneous Dataset. All simulations were run with identical physical and chemical configurations (Table 2), differing only in the erodibility dataset employed to isolate its effect on dust emissions and transport. For the August 2025 period, an additional simulation was performed, featuring the soil erodibility dataset developed by Li et al. (2023), to account for its performance in our domain of simulation. We simply refer to this simulation as LI2023, and its results can be observed in sections 3.1 and 3.2 of this work.

https://doi.org/10.5194/egusphere-2026-2127
Preprint. Discussion started: 22 April 2026

Dust emissions were computed online using the GOCART scheme, based on 10-m wind speed, soil moisture from the Noah land surface model, and the erodibility factor from the respective dataset, according to Eq. 1.

Table 3. Simulation periods covered in this study, together with their mean and maximum observed PM_{10} concentration values for the event. An asterisk (*) denotes a saturation of the observational instrument.

Simulation	Starting date	Ending date	Mean PM_{10}	Max. PM_{10}
2022-03	2022-03-11	2022-03-19	98.8	*1000.0
2022-07	2022-07-01	2022-07-08	35.8	133.0
2025-04	2025-04-26	2025-05-08	43.6	149.3
2025-08	2025-08-22	2025-08-31	52.0	204.5
2025-11	2025-11-08	2025-11-18	44.3	*1000.0

2.7 Statistical analysis

To quantify the model performance and the impact of using the high-resolution EROD-HR and SOILHD datasets, the following statistical metrics were calculated. On one hand, the Pearson correlation coefficient (R, Eq. 4) is used to assess the temporal agreement between observed and simulated concentrations. On the other hand, Mean Bias Error (MBE, Eq. 5) and Root Mean Square Error (RMSE, Eq. 6) are used to evaluate the accuracy and systematic bias of the model.

$$R_{XY} = \frac{\sum_{i=1}^{N}\left(X_i - \bar{X}\right)\left(Y_i - \bar{Y}\right)}{\sqrt{\sum_{i=1}^{N}\left(X_i - \bar{X}\right)^2}\sqrt{\sum_{i=1}^{N}\left(Y_i - \bar{Y}\right)^2}} \tag{4}$$

$$\mathrm{MBE} = \frac{1}{N}\sum_{i=1}^{N}\hat{X}_i - X_i \tag{5}$$

$$\mathrm{RMSE} = \sqrt{\frac{1}{N}\sum_{i=1}^{N}\left(\hat{X}_i - X_i\right)^2} \tag{6}$$

where $\hat{X}_i$ and X_i are the ith modeled and observed values, respectively, and $\overline{X}$ is the average value of all observations. 24-hour moving averages were also calculated to evaluate the ability of the model to capture daily dust variability, which is critical for air quality management and forecasting. The capability of the newly developed datasets to reproduce dust events in WRF-Chem simulations was assessed by computing metrics for several dust intrusion episodes spanning multiple seasons.

https://doi.org/10.5194/egusphere-2026-2127
Preprint. Discussion started: 22 April 2026

3 Results

3.1 Erodibility values and dust emission comparison

The new high-resolution soil erodibility fields for domains 1 and 3 are shown in Figs. 5 and 6, respectively. Table 4 summarizes the spatially averaged erodibility values for both domains, together with the total number of valid (non-zero) erodible grid cells for each dataset.

For domain 1, the average erodibility of the clay-silt classes, which dominate dust emissions in GOCART, is 0.0111 when all grid points are considered and 0.0474 when only source points are included. These values represent differences of -0.53% and -1.45%, respectively, relative to the original dataset. Despite the small change in domain-averaged erodibility, the spatial distribution differs markedly from the default field, with higher erodibility values concentrated in specific areas (Fig. 5). This redistribution, together with a reduction in the number of source grid cells from 20,620 to 18,251 (-11.5%), indicates that while the overall erosion potential of the domain remains nearly unchanged, the location of dust-emitting areas is substantially modified.

A more pronounced effect is observed over the RM (domain d03), where the number of source grid cells decreases from 18,458 (58.7% of the total) to 4,611 (14.7%). In contrast, the mean erodibility of these source points increases to 0.023, approximately one order of magnitude larger than in the original dataset. As shown in Fig. 6, the default CTRL configuration exhibits lower erodibility values distributed over broad areas, whereas the EROD-HR dataset produces a more heterogeneous pattern with localized high-erodibility regions. Nevertheless, the domain-averaged erodibility considering all grid points increases by only 0.39%, suggesting that the total dust uptake potential in domain d03 remains largely unchanged.

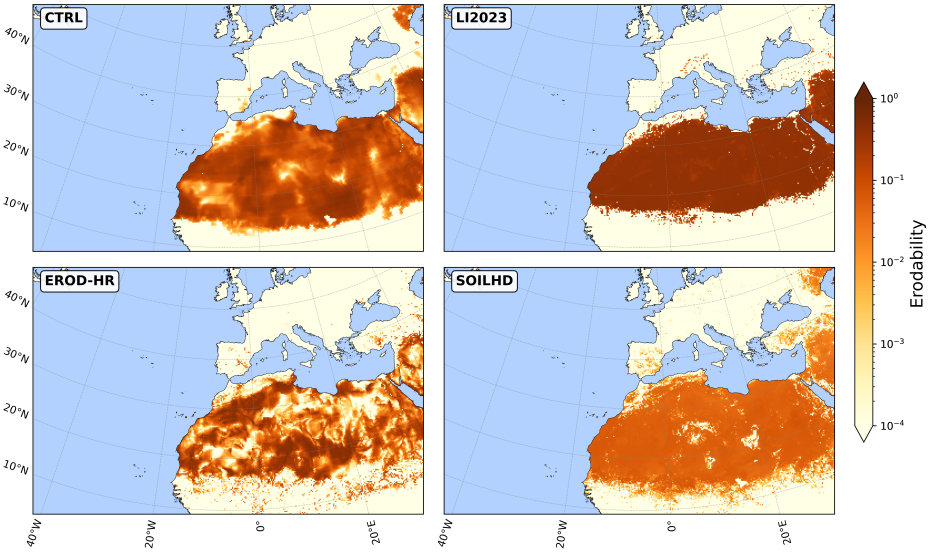

Figure 5. Soil erodibility fields (sand layer) of the 4 experiments (CTRL, LI2023, EROD-HR, and SOILHD) for domain d01.

https://doi.org/10.5194/egusphere-2026-2127
Preprint. Discussion started: 22 April 2026

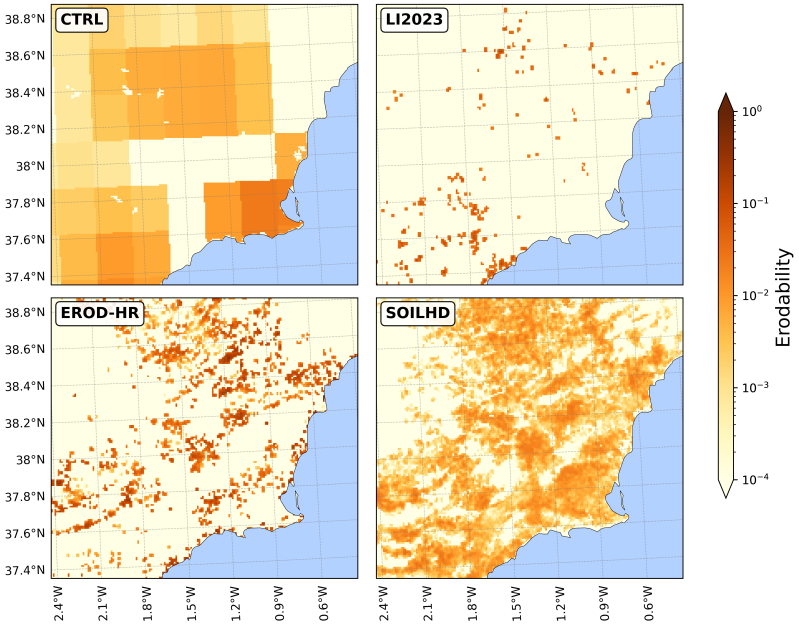

Figure 6. As Fig. 5, but for domain d03.

The behavior of the SOILHD dataset differs substantially from that of EROD-HR. For domain d01, the number of source grid cells increases to 22,045 and 22,020 for the silt and clay classes, respectively, representing increments of 6.9% and 6.8%. In contrast, the mean erodibility of these source points decreases to 0.0199 (silt) and 0.0185 (clay). Despite this reduction, the relative contributions of the silt and clay fractions to total erodibility amount to 25.3% and 23.5%, respectively, indicating that the assumption of an average sand content of 50% (i.e., a 50-25-25% sand-silt-clay composition) remains reasonable for domain d01. This behavior is also evident in Fig. 2, where the RGB representation is dominated by red tones associated with sandy soils over the Sahara Desert, while still revealing substantial spatial heterogeneity, with localized areas enriched in silt (green) and clay (blue).

The difference in the number of source points between the EROD-HR and SOILHD datasets highlights limitations associated with computing the source strength function S at local-scale resolution. In highly erodible regions of the Sahara Desert, this approach can yield very low or near-zero values of S, as illustrated in Fig. 5. The inclusion of soil texture information in SOILHD partially compensates for this effect by increasing the number of active source cells while preserving realistic erodibility magnitudes.

In contrast, the 50-25-25% soil texture assumption is not suitable for the RM (domain d03). As shown in Fig. 6, the SOILHD erodibility field exhibits a broader spatial distribution than EROD-HR, with lower values comparable to those of the CTRL configuration but confined to more localized areas at much higher spatial resolution. The total number of source points remains close to that of the original dataset (17,455, corresponding to a reduction of 4.7%). Fig. 3 further reveals a clear predominance of silt-rich soils across the region. This is consistent with the statistics reported in Table 4, which show that the silt fraction

https://doi.org/10.5194/egusphere-2026-2127
Preprint. Discussion started: 22 April 2026

Table 4. Erodibility statistics for domains d01 and d03. All-point and source-point mean erodibility values (silt and clay soil classes), as well as the number of total and dust source points, for each dataset, are shown. Exceptionally, for the SOILHD dataset, the clay and silt EROD-HR fields are not equivalent due to the heterogeneous distribution of the erodibility factor based on the specific soil class fraction available in each cell. Therefore, the total erodibility fractions of each separate soil class are displayed (%).

Domain	Value	CTRL	EROD-HR	SOILHD		LI2023
				Silt	Clay	
d01	**Mean (all)**	.0163	.0111	.0056 (25.3%)	.0052 (23.5%)	.0351
	Mean	.0619	.0474	.0199 (25.3%)	.0185 (23.5%)	.1663
	Source points	20620	18251	22045	22020	16512
	Total points	78273	78273	78273	78273	78273
d03	**Mean (all)**	.0014	.0034	.0038 (40.9%)	.0026 (27.9%)	.0005
	Mean	.0024	.0230	.0066 (40.0%)	.0046 (27.9%)	.0200
	Source points	18276	4603	17455	17406	784
	Total points	31450	31450	31450	31450	31450

accounts for approximately 40% of total erodibility (0.0066), while the clay fraction contributes about 28% (0.0046). Accordingly, a soil texture distribution of 30% sand, 40% silt, and 30% clay (30-40-30) appears more representative for domain d03.

As a consequence, the commonly assumed 50-25-25% soil distribution likely underestimates the availability of fine erodible particles in the RM, and thus the potential for dust emission. Changes in the relative contribution of dust emission by size bin are illustrated in Fig. 7. Emissions in the CTRL and EROD-HR experiments are nearly identical. In contrast, SOILHD exhibits a marked reduction in emissions from bin 1 (0-1 µm, clay), decreasing from 8.9% in CTRL to 6.3% (a reduction of 28.6%), accompanied by a slight increase in emissions from bins 2 to 4 (silt). These shifts in soil composition translate into changes in the size distribution of emitted dust particles and, consequently, in the $PM_{2.5}/PM_{10}$ ratio.

The coarsest size class (bin 5) is excluded from the analysis, as it comprises particles with effective diameters larger than 12 µm, exceeding the upper size threshold of PM_{10}.

https://doi.org/10.5194/egusphere-2026-2127
Preprint. Discussion started: 22 April 2026

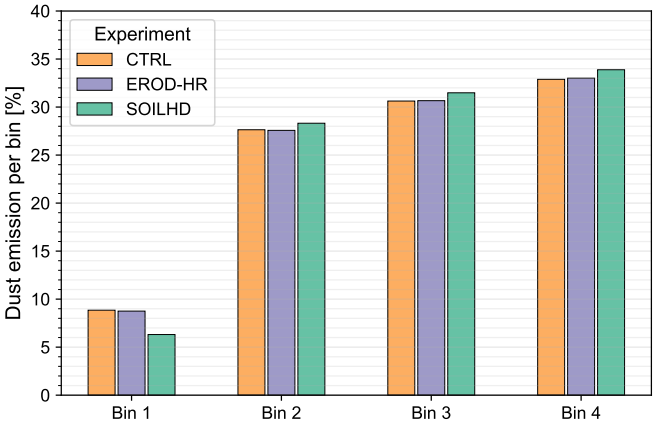

Figure 7. Dust emissions distribution by bin size for domain d03 during August 2025 is shown for the control (CTRL, orange), the high-resolution (EROD-HR, violet), and the high-resolution with soil mass fraction (SOILHD, green) experiments. Bin 1 (0.1–1.0 µm effective radius) represents clay particles, whereas bins 2 to 4 correspond to silt-sized particles, with effective radii ranges of 1.0–1.8 µm, 1.8–3.0 µm, and 3.0–6.0 µm, respectively. Bin 5 is not included in the analysis because it contains particles with effective diameters larger than 12 µm, which exceed the upper size threshold considered in the definition of PM_{10}.

Finally, average erodibility values were also computed for the previously published erodibility dataset described by Li et al. (2023), which integrates remote sensing products and soil properties to represent the spatial and temporal variability of dust source strength. For domain d01, the resulting mean erodibility values are 0.035 when averaged over all grid cells and 0.166 when considering only source points, indicating a spatially homogeneous erodibility pattern over the Sahara Desert. These values are approximately three times higher than those obtained with the CTRL dataset.

For domain d03, the mean erodibility at source points is 0.02, comparable to the EROD-HR dataset, but the number of active dust source cells is limited to only 784, corresponding to 2.5% of the total grid points. As a result, the domain-averaged erodibility is very low (0.0005). This configuration favors dust contributions dominated by transport from the parent domain, with negligible local dust uptake, which may lead to overestimated PM_{10} concentrations associated with convective transport (see Sec. 3.2). Such a behavior appears inconsistent with the known characteristics of the RM, which exhibits semi-arid conditions, low precipitation, and widespread areas of sparsely vegetated soils.

Additionally, the strong dependence of this kind of dataset on remote sensing retrievals may result in uncertainties and misvalues. For example, high erodibility values are observed over the Alps and the Pyrenees, two mountainous regions in central Europe and northern IP, respectively, characterized by rocky, snowy areas with negligible sand content, and therefore null dust uptaking potential.

Spatially averaged PM_{10} profiles were computed for domains d01 and d03 during the August 2025 event to examine the vertical distribution of PM_{10} (Fig. 9). For domain d01, the vertical PM_{10} profile shows a significant reduction in concentrations in the EROD-HR experiment relative to the CTRL one. This reduction is more pronounced in the SOILHD configuration, particularly near the surface, where the mean PM_{10} difference with respect to CTRL reaches -63.4 $\mu g\,m^{-3}$.

https://doi.org/10.5194/egusphere-2026-2127
Preprint. Discussion started: 22 April 2026

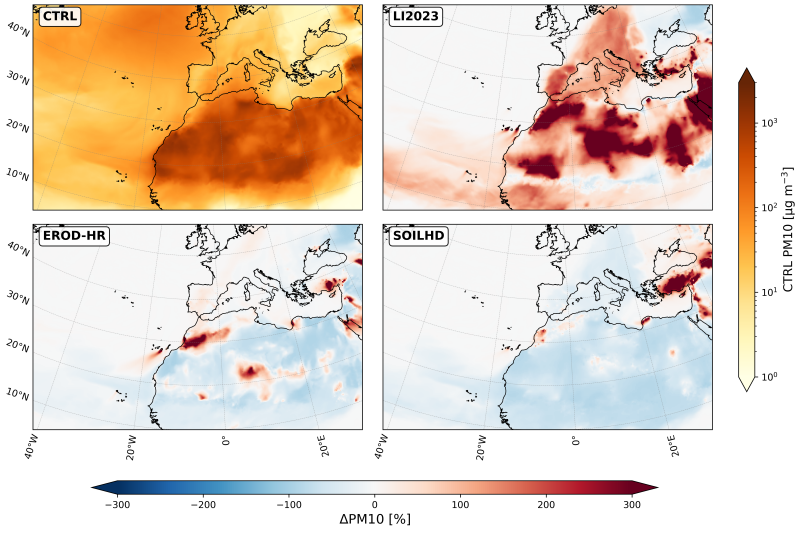

Figure 8. Temporal PM_{10} average for CTRL experiment during 2025-08 period (top left) and its relative difference with the other experiments.

Over the RM (domain d03), the vertical PM_{10} profiles obtained with CTRL and EROD-HR are nearly identical. In contrast, the SOILHD experiment exhibits lower PM_{10} concentrations than CTRL at all vertical levels, with a maximum difference of 47.0 $\mu g\,m^{-3}$ at model level 11 (approximately 750 hPa). This level also corresponds to the maximum PM_{10} concentrations, indicating that advective transport plays a dominant role in the vertical dust distribution over the region. As a result, modifications in the erodibility distribution of the parent domain propagate into significant differences in the simulated dust burden within the inner domain.

At the surface, the mean PM_{10} difference between SOILHD and CTRL amounts to 7.9 $\mu g\,m^{-3}$. Comparable behavior is observed for the remaining simulated periods. These results indicate that changes in soil mass fraction representation introduced by SOILHD affect both dust uplift and transport processes, leading to a modified vertical distribution of PM_{10}.

Additional simulations were performed using the erodibility dataset developed by Li et al. (2023) as the soil erodibility input (LI2023 experiment). The resulting vertical PM_{10} distributions for domains d01 and d03 indicate substantially higher concentrations than in all other experiments, with values that are two to three times larger than those obtained with the CTRL, EROD-HR, and SOILHD configurations. In domain d03, maximum PM_{10} concentrations exceed 250 $\mu g\,m^{-3}$, with surface values around 100 $\mu g\,m^{-3}$.

Similar behavior is observed for other simulated periods. For instance, during the 2022-07 event, a maximum PM_{10} concentration of 149.2 $\mu g\,m^{-3}$ is obtained with LI2023, whereas the CTRL, EROD-HR, and SOILHD experiments yield maxima ranging between 40.9 and 77.8 $\mu g\,m^{-3}$. This contrast suggests that the LI2023 dataset produces excessive dust emissions in the parent domain (d01) while generating very limited local dust uptake over the RM. Such a configuration is difficult to reconcile with the semi-arid conditions and the widespread presence of sparsely vegetated soils characteristic of the region.

https://doi.org/10.5194/egusphere-2026-2127
Preprint. Discussion started: 22 April 2026

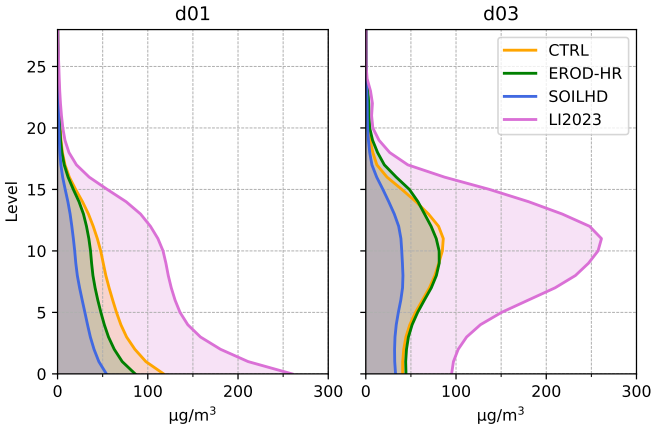

Figure 9. Vertical average PM_{10} distribution for domain 1 (left) and 3 (right) during period 2025–08 for the control (CTRL, red), the high-resolution (EROD-HR, green), the high-resolution with soil mass fraction (SOILHD, blue), and the dataset by Li et al. (2023) (LI2023, purple) experiments.

On this basis, the LI2023 experiment was excluded from the comparison with ground-based observations presented in the following section.

3.2 Comparison with ground-based measurements

Surface PM_{10} concentrations from all simulations were evaluated against observations from the SINQLAIR regional air quality monitoring network within the innermost domain (d03). Fig. 10 presents boxplots of the all-station correlation coefficients (left) and relative RMSE values (right) for each simulation period considered in this study. For most periods, the inclusion of the EROD-HR dataset and, in particular, the SOILHD configuration leads to a progressive improvement in model realism relative to the CTRL experiment.

For example, during the 2022-07 period, CTRL underestimates PM_{10} concentrations at six of the eight stations, yielding an average mean bias error (MBE) of -4.05 $\mu g\,m^{-3}$ and RMSE values frequently exceeding 20 $\mu g\,m^{-3}$. In addition, only 50% of the stations exhibit statistically significant correlations (p-value < 0.01). Simulations using the EROD-HR dataset tend to either maintain this underestimation or slightly overestimate PM_{10}, depending on the station, with an average RMSE of 18.56 $\mu g\,m^{-3}$; only two stations (CAR and ESC) exceed 20 $\mu g\,m^{-3}$. The SOILHD experiment further reduces the errors and provides a more accurate representation of the temporal structure of the dust peak.

For the 2022–03 dust event, characterized by record-breaking and persistent PM_{10} concentrations over the RM, the improvement achieved with SOILHD is even more pronounced relative to CTRL and EROD-HR. The average correlation coefficient increases from 0.43 to 0.58, with a maximum value of 0.70(compared to 0.55 in CTRL), while the average RMSE decreases substantially from 275.5 to 145.4 $\mu g\,m^{-3}$, which poses a relative difference of -117.4%.

https://doi.org/10.5194/egusphere-2026-2127
Preprint. Discussion started: 22 April 2026

Overall, the SOILHD configuration yields the highest average correlation values in four out of the five simulated periods (with the remaining case, 2022–07, still outperforming CTRL) and the lowest RMSE values in three out of five periods (except for 2025–11, and 2022-07, a period which exhibits the lowest PM_{10} concentrations when the RMSE values are almost identical). Both the EROD-HR and SOILHD experiments consistently produce statistically significant correlation coefficients (p-value < 0.01), confirming the robustness of the improvements introduced by the high-resolution erodibility datasets.

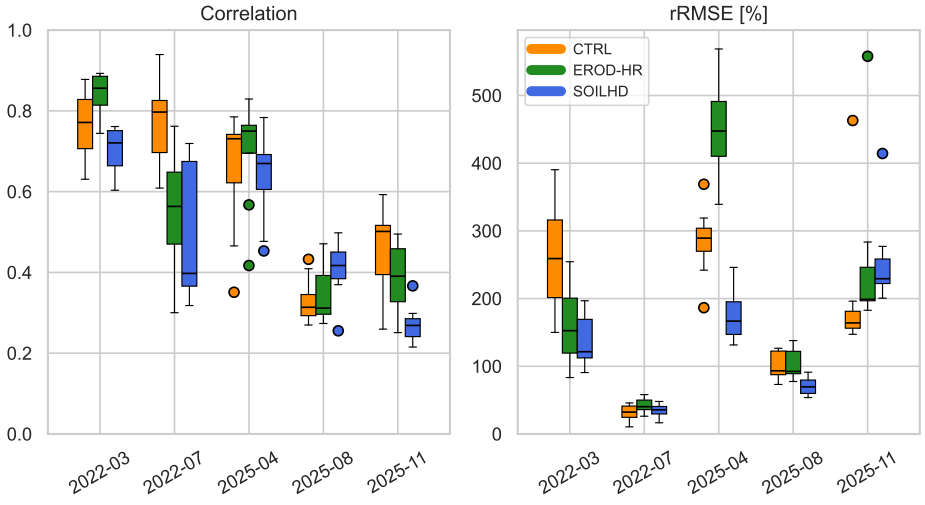

Figure 10. Boxplots for Correlation (left) and relative RMSE (right) distributions for every simulation period by experiment (CTRL, orange; EROD-HR, green; and SOILHD, blue).

The August 2025 case was examined in greater detail, as it represents a summer dust episode characterized by the combined influence of local dust uplift and convective transport, a situation in which the physical configuration of the erodibility field is particularly influential. Fig. 11 presents surface PM_{10} observational (OBS) and modeled (CTRL, EROD-HR, and SOILHD) time series (dashed lines) for the 2025-08 period, obtained by bilinear interpolation of model output to the geographic coordinates of the SINQLAIR monitoring stations. In addition, 24-hour moving averages (24MA) are shown for all series (solid lines), both to improve clarity and visualization and because 24-hour averaging is a standard metric in air quality analysis and forecasting. Complementary PM_{10} boxplots summarizing the distribution at each station and for every dataset are also included. For a more detailed inspection of individual station time series, Fig. B1 is provided.

https://doi.org/10.5194/egusphere-2026-2127
Preprint. Discussion started: 22 April 2026

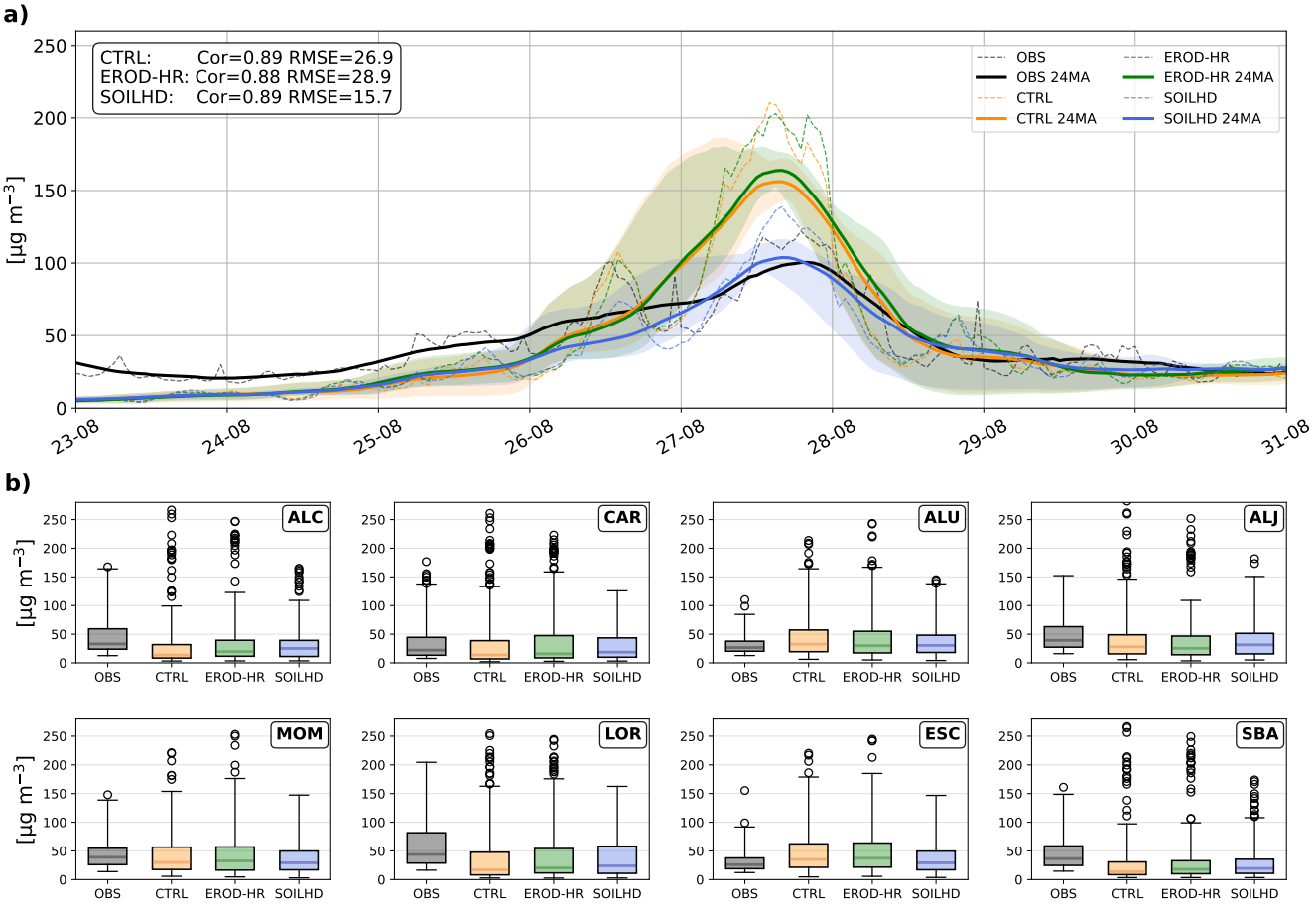

Figure 11. a) Site-averaged PM_{10} time series (dashed lines) and 24-hour moving average series (solid lines) for observations (black) and CTRL (orange), EROD-HR (green), and SOILHD (blue) experiments obtained by bilinearly interpolating the model experiments to each SINQLAIR station location. For a given dataset series, the PM_{10} span across all stations is also represented (light colors). The metrics of every dataset are displayed in the top-left corner of the plot. b) Boxplots with the interpolated PM_{10} values for every station and dataset. Outlier values are represented with circles

Overall, the SOILHD configuration provides the best agreement with observations at most monitoring stations, particularly during the main dust event of 27–28 August, when it successfully captures peak PM_{10} concentrations at multiple sites. From 26 August onwards, the 24-hour moving-average (24MA) observational series remains within the envelope defined by the individual station time series simulated with SOILHD, indicating that this configuration produces PM_{10} concentrations which are representative of the observed inter-station variability. In addition, SOILHD closely matches the observations, reproducing both mean and peak PM_{10} values at most locations.

In contrast, both the CTRL and EROD-HR experiments substantially overestimate PM_{10} concentrations across all stations, particularly during high concentration episodes. For instance, at the San Basilio (SBA) station, CTRL and EROD-HR simu-

https://doi.org/10.5194/egusphere-2026-2127
Preprint. Discussion started: 22 April 2026

lations reach peak values exceeding 250 $\mu g\,m^{-3}$, whereas the observed maximum is approximately 150 $\mu g\,m^{-3}$. It is noted, however, that the simulations do not include anthropogenic emission sources such as nitrogen oxides (NO_x), sulfur dioxide (SO_2), or black carbon (BC), which may contribute to elevated PM_{10} concentrations over longer timescales. Although all configurations yield similar correlation coefficients (0.89), the SOILHD experiment exhibits a substantially lower RMSE (15.7 $\mu g\,m^{-3}$), highlighting its superior quantitative performance.

A closer examination of the individual time series at each monitoring station (Table 5) confirms that the SOILHD configuration provides the best overall performance. SOILHD yields lower RMSE values at 7 out of 8 stations, with an average reduction of 10.9 $\mu g\,m^{-3}$ relative to the CTRL experiment. Although all configurations exhibit high correlation coefficients at most sites, SOILHD attains the highest correlation at five of the eight stations, with an average value of 0.77.

Table 5. Statistical parameters (correlation and RMSE) for the time series of the three different experiments during the period starting on 2025-08-22. Time series for each location were obtained by bilinearly interpolating every model output to its respective ground station location. All correlations are significant (p-value < 0.01). RMSE units are $\mu g\,m^{-3}$.

Cor.	ALC	CAR	ALU	ALJ	MOM	LOR	ESC	SBA	Mean
CTRL	0.85	0.88	0.78	0.57	0.71	0.88	0.56	0.84	**0.76**
EROD-HR	0.85	0.90	0.76	0.55	0.68	0.90	0.52	0.84	**0.75**
SOILHD	0.85	0.89	0.80	0.60	0.73	0.86	0.54	0.86	**0.77**
RMSE	**ALC**	**CAR**	**ALU**	**ALJ**	**MOM**	**LOR**	**ESC**	**SBA**	**Mean**
CTRL	34.0	33.6	35.6	44.2	31.5	34.9	40.4	34.8	**36.1**
EROD-HR	34.3	29.1	39.4	45.5	37.4	31.7	45.6	34.2	**37.2**
SOILHD	22.3	20.5	21.0	28.2	22.6	35.6	27.4	24.1	**25.2**

When switching to the new high-resolution erodibility datasets, near-coastal stations (ALU, ALJ, ESC, and MOM) exhibit a weaker, yet still statistically significant, response in terms of correlation, together with a marked improvement in RMSE relative to observations, with the exception of ESC. At these sites, all model configurations tend to overestimate PM_{10} concentrations, suggesting an overestimation of local dust source strength and/or excessive recirculation within the model domain.

The ESC station represents a particular case, as its observed PM_{10} variability is substantially higher than at any other site. This behavior may be partly explained by the contribution of sea-salt aerosols to PM_{10} levels and by the proximity of the station to the Escombreras combined-cycle power plant, a known source of black carbon, nitrates, sulfates, and other anthropogenic pollutants not explicitly represented in the simulations. Nevertheless, the model is able to partially reproduce the observed variability at ESC, particularly in the EROD-HR and SOILHD experiments. These configurations also capture the magnitude of several PM_{10} peaks, most notably during the dust outbreak of 27–28 August. Among the simulations, the modeled time series transitions from a slight overestimation in the SOILHD experiment to a more pronounced overestimation in CTRL and EROD-HR.

For inland stations (ALC, CAR, LOR, and SBA), CTRL and EROD-HR exhibit nearly identical behavior, substantially overestimating observed PM_{10} concentrations, especially during the peak associated with the 27–28 August dust event. In

https://doi.org/10.5194/egusphere-2026-2127
Preprint. Discussion started: 22 April 2026

contrast, the SOILHD experiment shows a remarkable agreement with observations, accurately reproducing both the timing and magnitude of the PM_{10} maximum. For instance, at Alcantarilla (ALC), SOILHD simulates a maximum concentration of 165.1 $\mu g\,m^{-3}$ on 27 August, in close agreement with the observed value of 167.6 $\mu g\,m^{-3}$ (relative error of 1.5%). In comparison, CTRL and EROD-HR yield maxima of 266.6 and 247.1 $\mu g\,m^{-3}$, corresponding to errors of 59.1% and 47.4%, respectively. The only notable exception to the overall pattern is observed at the Lorca (LOR) station, where both CTRL and EROD-HR simulations more closely capture the observed peak PM10 concentrations. In contrast, SOILHD consistently exhibits a negative bias throughout the study period. This discrepancy is likely attributable to the strong influence of anthropogenic pollution at LOR, which is not represented in the current simulations. Local industrial activity and traffic emissions, each with distinct diurnal cycles, may contribute an additional PM10 background that is absent from the model, resulting in systematic underestimation in highly polluted areas.

To further illustrate these dynamics, Fig. C1 presents the time series of PM10 and accumulated dust for all eight stations during the 2025–08 period. For coastal stations (ALU, ALJ, MOM, and ESC), it is evident that the accumulated dust concentrations alone cannot account for the modeled PM10 levels, indicating a substantial contribution from marine salt to the natural-origin PM10 fraction (the only component represented in the present simulations). Conversely, at some stations, namely ALC, ALJ, MOM, LOR, ESC, and SBA, SOILHD systematically underestimates the observed PM10 concentrations. The observed deviations can be attributed to a combination of external PM_{10} sources specific to each location, such as heavy traffic (ALC, MOM, LOR, SBA), industrial emissions (ALC, MOM, ESC), and agricultural activities such as soil tilling (ALJ).

Based on the discrepancy between observations and the SOILHD experiment, which performs well in low-pollution environments, this anthropogenic contribution can be estimated to range between approximately 25 and 50 $\mu g\,m^{-3}$. This interpretation is further supported by results at Caravaca (CAR), a station located in the northwestern part of the RM, where anthropogenic influences are minimal. At this site, SOILHD clearly provides the best agreement with observations. It is important to note that the primary objective of this study is to evaluate the performance of the new erodibility database, rather than to develop an operational air-quality forecasting system. The incorporation of anthropogenic emission inventories is therefore beyond the scope of the present work, but will be addressed in future simulations.

4 Conclusions

This study presents the development and evaluation of two new high-resolution soil erodibility datasets implemented within the WRF-Chem model coupled with the GOCART aerosol scheme to improve the representation of mineral dust emissions and transport over regions characterized by complex topography and heterogeneous surface properties. To this end, GMTED2010 topographic elevation data were combined with the MODIS 20-category land-use classification to produce a physically consistent global dataset at 5 km resolution (EROD-HR). To further refine the simulations, a high-resolution soil texture dataset from ISRIC SoilGrids (250 m resolution), together with a LCZ-based global land category map at 7.5-arcsecond resolution, was incorporated to generate an enhanced dataset including explicit mass fractions of sand, silt, and clay (SOILHD). The resulting

https://doi.org/10.5194/egusphere-2026-2127
Preprint. Discussion started: 22 April 2026

datasets substantially modify the spatial distribution of potential dust sources relative to the default WRF-Chem erodibility field (CTRL).

The analysis of the new erodibility fields indicates that, although the overall mean erodibility remains comparable to that of the default dataset, the spatial configuration of dust emission sources changes markedly. Over the RM (d03), the number of active source points is reduced, while their mean erodibility increases, resulting in more concentrated and physically consistent dust source regions. This refinement leads to a more realistic spatial distribution of dust emissions, limiting the excessive spatial spreading of sources while enhancing emissions in areas with genuinely high erosion potential. Such a refined distribution better captures the natural heterogeneity of arid and semi-arid regions, such as southeastern Spain, where coarse-resolution datasets tend to diffuse or misrepresent dust source areas. The inclusion of explicit soil mass fraction layers in the SOILHD configuration further strengthens the physical basis of the dataset by distinguishing between sand, silt, and clay contributions, thereby modulating dust lifting intensity without artificially increasing total emission fluxes.

When implemented within WRF-Chem, the SOILHD configuration yields substantial improvements in the reproduction of observed PM_{10} concentrations. A comparative analysis covering all simulated periods (Table 3) was conducted against a regional air quality observational dataset for the RM, comprising eight monitoring stations with a native temporal resolution of 10 minutes. The SOILHD configuration achieves the highest correlation and lowest RMSE values in four out of five simulated periods (80%), with particularly strong performance during the August 2025 dust episode. This event, characterized by the combined influence of local dust uplift and convective transport, is especially sensitive to the physical configuration of the erodibility field.

Vertical profile analyses indicate a more balanced partition between local and advected dust contributions under the SOILHD configuration, resulting in more realistic surface concentrations and vertical gradients compared to the default setup. In contrast, simulations employing the erodibility dataset proposed by Li et al. (2023) (LI2023 experiment) produce unrealistically high PM_{10} levels, consistent with an overestimation of dust emission potential over highly arid regions such as the Sahara Desert. Overall, the refined EROD-HR and SOILHD datasets enhance the realism of the simulations, with SOILHD emerging as the most robust configuration. By incorporating physically consistent surface parameters, the model attains both improved quantitative agreement and a more realistic representation of PM_{10} variability over the IP.

The introduction of the new erodibility datasets results in a differentiated model response between coastal and inland monitoring stations. At near-coastal sites, the use of high-resolution erodibility fields leads to a slightly weaker, yet still statistically significant, correlation with observations, while producing a substantial improvement in RMSE at most stations. Despite this improvement, all model configurations tend to overestimate PM_{10} at these locations, indicating a likely overestimation of local dust source strength and/or an excessive representation of recirculation processes within the model domain.

For inland stations, the benefits of the high-resolution soil datasets are more pronounced. The CTRL and EROD-HR experiments exhibit nearly identical behavior, substantially overestimating PM_{10} concentrations, particularly during the main dust peak on 27–28 August. In contrast, the SOILHD configuration shows a markedly improved agreement with observations, accurately reproducing both the timing and magnitude of the PM_{10} peak. At the Alcantarilla (ALC) station, for example, SOILHD

https://doi.org/10.5194/egusphere-2026-2127
Preprint. Discussion started: 22 April 2026

reproduces the observed maximum concentration with an error below 2%, whereas CTRL and EROD-HR overestimate the peak by more than 45–60%.

The Lorca (LOR) station represents a notable exception to this inland pattern. At this site, CTRL and EROD-HR provide a closer match to the observed peak, while SOILHD exhibits a systematic negative bias throughout the period. This behavior is likely related to the strong influence of anthropogenic emissions associated with industrial activity and traffic, which introduce a pronounced diurnal cycle not represented in the current simulations. The discrepancy between observations and the SOILHD results suggests an anthropogenic PM_{10} contribution on the order of 25—50 $\mu g\,m^{-3}$, consistent with the differences observed relative to stations such as Caravaca (CAR), where anthropogenic influence is minimal and SOILHD yields the best overall performance.

This work shows that the incorporation of a high-resolution erodibility field substantially improves the representation of mineral dust emissions and transport in WRF-Chem simulations using the GOCART scheme. A more realistic characterization of soil texture and erodibility leads to significant improvements in the simulation of dust-related PM_{10} concentrations, particularly over inland areas and environments with limited anthropogenic influence. Although the absence of anthropogenic emissions constrains model performance at heavily polluted locations, this limitation does not compromise the primary objective of this study, namely the assessment of the added value provided by the new erodibility datasets.

The high-resolution SOILHD dataset notably enhances the spatial and temporal consistency of dust emission simulations, enabling a more realistic representation of both large-scale Saharan dust transport and fine-scale local dust uplift processes over the southern IP. These results suggest that both operational and research-oriented dust forecasting systems could benefit from the adoption of enhanced erodibility fields. Future developments will focus on incorporating temporally varying vegetation parameters to account for seasonal changes in surface cover, extending the validation framework to other dust-prone regions worldwide, and integrating anthropogenic emission inventories in order to advance toward a fully coupled and robust air-quality modeling framework.

https://doi.org/10.5194/egusphere-2026-2127
Preprint. Discussion started: 22 April 2026

Appendix A: SINQLAIR Stations Map

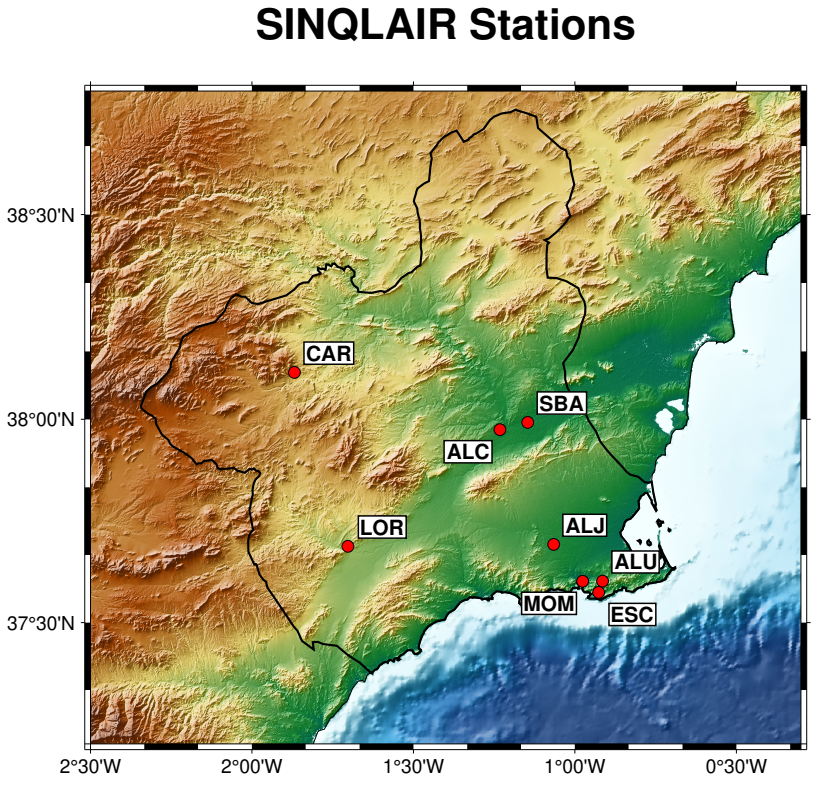

Figure A1. Distribution of SINQLAIR stations network

https://doi.org/10.5194/egusphere-2026-2127
Preprint. Discussion started: 22 April 2026

Appendix B: Time series by station (2025–08)

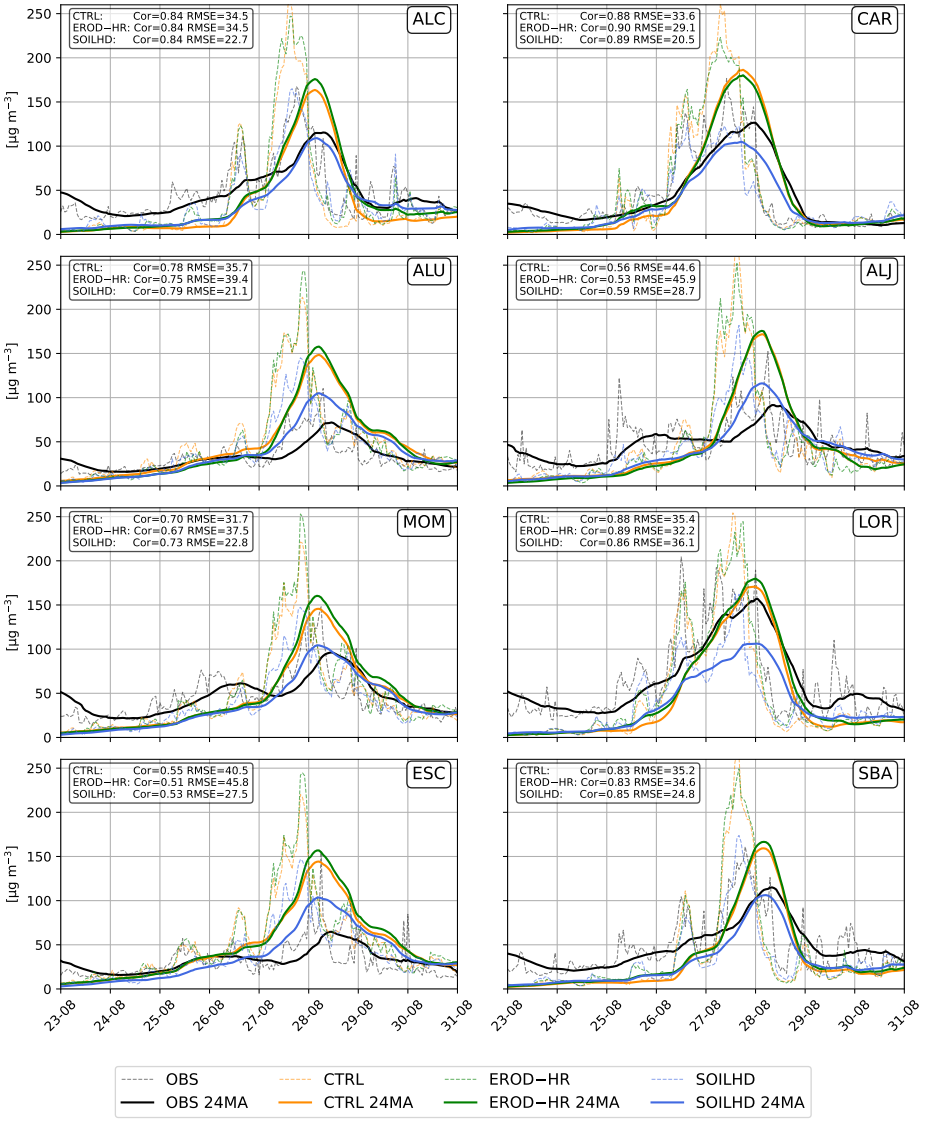

Figure B1. PM_{10} time series for all stations.

https://doi.org/10.5194/egusphere-2026-2127
Preprint. Discussion started: 22 April 2026

Appendix C: Stacked Dust series (2025–08)

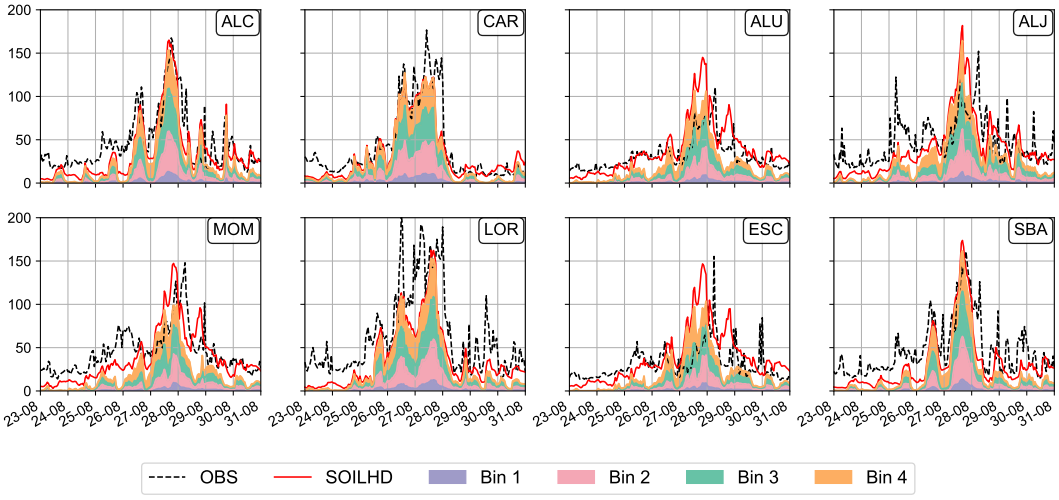

Figure C1. Dust-stacked time series for all stations by GOCART dust bins.

https://doi.org/10.5194/egusphere-2026-2127
Preprint. Discussion started: 22 April 2026

Code and data availability. The datasets and software used and produced in this study are publicly available through Zenodo:

- EROD-HR – A High Resolution Global Dust Erodibility Dataset (Segado-Moreno et al., 2026a), DOI: https://doi.org/10.5281/zenodo.18594482, version 1.0.0, provides global high-resolution information on soil erodibility for dust emission modeling.
- SOILHD – Soil-Type Heterogeneous Erodibility Dataset (Segado-Moreno et al., 2026b), DOI: https://doi.org/10.5281/zenodo.18596292, version 1.0.0, offers a 1 km resolution representation of dust erodibility potential considering a heterogeneous soil type classification.
- EROD Tuner (Segado-Moreno and Montavez, 2026), DOI: https://doi.org/10.5281/zenodo.18606994, version 1.0.0, is a preprocessing utility that enables flexible modification of the soil erodibility factor (EROD) in the WRF Preprocessing System (WPS).

Both datasets and the source code can be directly accessed and downloaded via the provided DOI links.

Author contributions. L. C. Segado-Moreno contributed to all stages of the study, including the initial conceptualization, data acquisition and processing, production and analysis of results, interpretation of findings, manuscript writing, and subsequent revisions. J. P. Montávez participated in the development of the research concept, contributed to the interpretation and discussion of the results, and was involved in the revision of the manuscript. G. Garnés-Morales, E. Raluy-López, and P. Jiménez-Guerrero contributed to the critical review and editing of the manuscript. All authors read and approved the final version of the paper.

Competing interests. One of the co-authors, Pedro Jiménez-Guerrero, is a member of the editorial board of Atmospheric Chemistry and Physics. The authors declare that no other competing interests are present.

Acknowledgements. Funding support for this work was provided by the ECCE (PID2020-115693RB-I00), ARUBA (PID2023-149080OB-I00) projects from Ministerio de Ciencia e Innovación/Agencia Estatal de Investigación, Spain, and the European Regional Development Fund (ERDF/FEDER), and the project INSIEME (FSRM/10.13039/100007801). L.C. Segado-Moreno thanks the predoctoral contract FPI (PRE2021-099236) from the Spanish Ministry of Science and Innovation.

The authors acknowledge that artificial intelligence-based tools were used in the preparation of this manuscript to assist in the drafting and refinement of parts of the Abstract and Introduction. These tools were used solely for language improvement and text structuring purposes, and all scientific content, interpretations, and conclusions were developed, reviewed, and validated by the authors.

https://doi.org/10.5194/egusphere-2026-2127
Preprint. Discussion started: 22 April 2026

References

Beloconi, A. and Vounatsou, P.: Revised EU and WHO air quality thresholds: Where does Europe stand?, Atmospheric Environment, 314, 120 110, https://doi.org/10.1016/j.atmosenv.2023.120110, 2023.

Chen, F. and Dudhia, J.: Coupling an advanced land surface–hydrology model with the Penn State–NCAR MM5 modeling system. Part I: Model implementation and sensitivity, Monthly weather review, 129, 569–585, https://doi.org/10.1175/1520-0493(2001)129<0587:CAALSH>2.0.CO;2, 2001.

Chung, C. E.: Aerosol direct radiative forcing: a review, Atmospheric aerosols—regional characteristics—chemistry and physics, pp. 379–394, https://doi.org/10.5772/50248, 2012.

Danielson, J. and Gesch, D.: Global multi-resolution terrain elevation data 2010 (GMTED2010), Tech. rep., U.S. Department of the Interior, https://doi.org/10.3133/ofr20111073, 2011.

Darmenova, K., Sokolik, I. N., Shao, Y., Marticorena, B., and Bergametti, G.: Development of a physically based dust emission module within the Weather Research and Forecasting (WRF) model: Assessment of dust emission parameterizations and input parameters for source regions in Central and East Asia, Journal of Geophysical Research: Atmospheres, 114, https://doi.org/10.1029/2008JD011236, 2009.

DeFries, R., Townshend, J., and Hansen, M.: Continuous fields of vegetation characteristics at the global scale at 1-km resolution, Journal of Geophysical Research: Atmospheres, 104, 16 911–16 923, https://doi.org/10.1029/1999JD900057, 1999.

Demuzere, M., Kittner, J., Martilli, A., Mills, G., Moede, C., Stewart, I. D., Van Vliet, J., and Bechtel, B.: A global map of Local Climate Zones to support earth system modelling and urban scale environmental science, Earth System Science Data Discussions, 2022, 1–57, https://doi.org/10.5194/essd-14-3835-2022, 2022.

Demuzere, M., Kittner, J., Martilli, A., Mills, G., Moede, C., Stewart, I. D., van Vliet, J., and Bechtel, B.: Global map of Local Climate Zones, https://doi.org/10.5281/zenodo.8419340, 2023.

Eltahan, M., Shokr, M., and Sherif, A. O.: Simulation of severe dust events over Egypt using tuned dust schemes in weather research forecast (WRF-Chem), Atmosphere, 9, 246, https://doi.org/10.3390/atmos9070246, 2018.

Friedl, M., McIver, D., Hodges, J., Zhang, X., Muchoney, D., Strahler, A., Woodcock, C., Gopal, S., Schneider, A., Cooper, A., Baccini, A., Gao, F., and Schaaf, C.: Global land cover mapping from MODIS: algorithms and early results, Remote Sensing of Environment, 83, 287–302, https://doi.org/10.1016/S0034-4257(02)00078-0, the Moderate Resolution Imaging Spectroradiometer (MODIS): a new generation of Land Surface Monitoring, 2002.

Garnés-Morales, G., Montávez, J. P., Halifa-Marín, A., and Jiménez-Guerrero, P.: Role of aerosols on atmospheric circulation in regional climate Experiments over Europe, Atmosphere, 14, 491, https://doi.org/10.3390/atmos14030491, 2023.

Garnés-Morales, G., Tortosa, J., Jiménez-Guerrero, P., Gil-Guirado, S., García-Fernández, E., and Montávez, J. P.: Assessing the effects of compound events of temperature and air pollution on weekly mortality in Spain using random forests, Weather and Climate Extremes, p. 100816, https://doi.org/10.1016/j.wace.2025.100816, 2025.

Georgiou, G. K., Christoudias, T., Proestos, Y., Kushta, J., Pikridas, M., Sciare, J., Savvides, C., and Lelieveld, J.: Evaluation of WRF-Chem model (v3.9.1.1) real-time air quality forecasts over the Eastern Mediterranean, Geoscientific Model Development, 15, 4129–4146, https://doi.org/10.5194/gmd-15-4129-2022, 2022.

https://doi.org/10.5194/egusphere-2026-2127
Preprint. Discussion started: 22 April 2026

Ginoux, P., Chin, M., Tegen, I., Prospero, J. M., Holben, B., Dubovik, O., and Lin, S.-J.: Sources and distributions of dust aerosols simulated with the GOCART model, Journal of Geophysical Research: Atmospheres, 106, 20 255–20 273, https://doi.org/10.1029/2000JD000053, 2001.

Grell, G. A.: Prognostic evaluation of assumptions used by cumulus parameterizations, Monthly weather review, 121, 764–787, https://doi.org/10.1175/1520-0493(1993)121<0764:PEOAUB>2.0.CO;2, 1993.

Grell, G. A. and Dévényi, D.: A generalized approach to parameterizing convection combining ensemble and data assimilation techniques, Geophysical Research Letters, 29, 38–1, https://doi.org/10.1029/2002GL015311, 2002.

Grell, G. A., Peckham, S. E., Schmitz, R., McKeen, S. A., Frost, G., Skamarock, W. C., and Eder, B.: Fully coupled "online" chemistry within the WRF model, Atmospheric environment, 39, 6957–6975, https://doi.org/10.1016/j.atmosenv.2005.04.027, 2005.

Hengl, T., Mendes de Jesus, J., Heuvelink, G. B., Ruiperez Gonzalez, M., Kilibarda, M., Blagotić, A., Shangguan, W., Wright, M. N., Geng, X., Bauer-Marschallinger, B., et al.: SoilGrids250m: Global gridded soil information based on machine learning, PLoS one, 12, e0169 748, https://doi.org/10.1371/journal.pone.0169748, 2017.

Hersbach, H., Bell, B., Berrisford, P., Biavati, G., Horányi, A., Muñoz Sabater, J., Nicolas, J., Peubey, C., Radu, R., Rozum, I., et al.: ERA5 hourly data on pressure levels from 1940 to present. Copernicus Climate Change Service (C3S) Climate Data Store (CDS). (Accessed on 2025-02-01), 2018.

Hong, S.-Y., Noh, Y., and Dudhia, J.: A new vertical diffusion package with an explicit treatment of entrainment processes, Monthly weather review, 134, 2318–2341, https://doi.org/10.1175/MWR3199.1, 2006.

Iacono, M. J., Delamere, J. S., Mlawer, E. J., Shephard, M. W., Clough, S. A., and Collins, W. D.: Radiative forcing by long-lived greenhouse gases: Calculations with the AER radiative transfer models, Journal of Geophysical Research: Atmospheres, 113, https://doi.org/10.1029/2008JD009944, 2008.

Jerez, S., Palacios-Peña, L., Gutiérrez, C., Jiménez-Guerrero, P., López-Romero, J. M., Pravia-Sarabia, E., and Montávez, J. P.: Sensitivity of surface solar radiation to aerosol–radiation and aerosol–cloud interactions over Europe in WRFv3.6.1 climatic runs with fully interactive aerosols, Geoscientific Model Development, 14, 1533–1551, https://doi.org/10.5194/gmd-14-1533-2021, 2021.

Jiménez, P. A., Dudhia, J., González-Rouco, J. F., Navarro, J., Montávez, J. P., and García-Bustamante, E.: A revised scheme for the WRF surface layer formulation, Monthly weather review, 140, 898–918, https://doi.org/10.1175/MWR-D-11-00056.1, 2012.

Jin, J., Segers, A., Liao, H., Heemink, A., Kranenburg, R., and Lin, H.: Source backtracking for dust storm emission inversion using an adjoint method: case study of Northeast China, Atmospheric Chemistry and Physics, https://doi.org/10.5194/acp-20-15207-2020, 2020.

Johnson, B., Shine, K., and Forster, P.: The semi-direct aerosol effect: Impact of absorbing aerosols on marine stratocumulus, Quarterly Journal of the Royal Meteorological Society, 130, 1407–1422, https://doi.org/10.1256/qj.03.61, 2004.

Knippertz, P. and Todd, M.: Mineral dust aerosols over the Sahara: Meteorological controls on emission and transport and implications for modeling, Reviews of Geophysics, 50, https://doi.org/10.1029/2011rg000362, 2012.

Kok, J., Adebiyi, A., Albani, S., Balkanski, Y., Checa-Garcia, R., Chin, M., Colarco, P., Hamilton, D., Huang, Y., Ito, A., Klose, M., Leung, D. M., Li, L., Mahowald, N., Miller, R. L., Obiso, V., García-Pando, C. P., Rocha-Lima, A., Wan, J. S., and Whicker, C.: Improved representation of the global dust cycle using observational constraints on dust properties and abundance., Atmospheric chemistry and physics, 21 10, 8127–8167, https://doi.org/10.5194/acp-2020-1131, 2020.

Kok, J. F., Ward, D. S., Mahowald, N. M., and Evan, A. T.: Global and regional importance of the direct dust-climate feedback, Nature communications, 9, 241, https://doi.org/10.1038/s41467-017-02620-y, 2018.

https://doi.org/10.5194/egusphere-2026-2127
Preprint. Discussion started: 22 April 2026

Lee, J. A., Jiménez, P. A., Kumar, R., and He, C.: Impact of direct insertion of SMAP soil moisture retrievals in WRF-Chem for dust storm events in the western US, Atmospheric Environment, 321, 120 349, https://doi.org/10.1016/j.atmosenv.2024.120349, 2024.

Lee, J.-H., Lee, S.-H., and Cho, J. H.: A novel method for detecting natural dust source regions using satellite and ground-based measurements, Atmospheric Environment, 344, 121 024, https://doi.org/10.1016/j.atmosenv.2024.121024, 2025.

LeGrand, S. L., Polashenski, C., Letcher, T. W., Creighton, G. A., Peckham, S. E., and Cetola, J. D.: The AFWA dust emission scheme for the GOCART aerosol model in WRF-Chem v3. 8.1, Geoscientific Model Development, 12, 131–166, https://doi.org/10.5194/gmd-12-131-2019, 2019.

Li, H. and Wang, C.: Impact of dust radiation effect on simulations of temperature and wind–A case study in Taklimakan Desert, Atmospheric Research, 273, 106 163, https://doi.org/10.1016/j.atmosres.2022.106163, 2022.

Li, H., Wang, C., Wang, M., Liu, Z., Mamtimin, A., and Pan, X.: A new dataset of erodibility in dust source for WRF-Chem model based on remote sensing and soil texture-Application and Validation, Atmospheric Environment, 315, 120 156, https://doi.org/10.1016/j.atmosenv.2023.120156, 2023.

López-Cayuela, M.-A., Córdoba-Jabonero, C., Sicard, M., Abril-Gago, J., Salgueiro, V., Comerón, A., Granados-Muñoz, M. J., Costa, M. J., Muñoz Porcar, C., Bravo-Aranda, J. A., Bortoli, D., Rodríguez-Gómez, A., Alados-Arboledas, L., and Guerrero-Rascado, J. L.: Fine and coarse dust radiative impact during an intense Saharan dust outbreak over the Iberian Peninsula – short-wave direct radiative effect, Atmospheric Chemistry and Physics, 25, 3213–3231, https://doi.org/10.5194/acp-25-3213-2025, 2025.

Mahowald, N., Ballantine, J., Feddema, J., and Ramankutty, N.: Global trends in visibility: implications for dust sources, Atmospheric Chemistry and Physics, 7, 3309–3339, https://doi.org/10.5194/acp-7-3309-2007, 2007.

Masson-Delmotte, V., Zhai, P., Pirani, A., Connors, S. L., Péan, C., Berger, S., Caud, N., Chen, Y., Goldfarb, L., Gomis, M., et al.: Climate change 2021: the physical science basis, Contribution of working group I to the sixth assessment report of the intergovernmental panel on climate change, 2, 2391, https://doi.org/10.1017/9781009157896, 2021.

Morrison, H., Curry, J., and Khvorostyanov, V.: A new double-moment microphysics parameterization for application in cloud and climate models. Part I: Description, Journal of the atmospheric sciences, 62, 1665–1677, https://doi.org/10.1175/JAS3446.1, 2005.

Palacios-Peña, L., Lorente-Plazas, R., Montávez, J. P., and Jiménez-Guerrero, P.: Saharan dust modeling over the Mediterranean basin and Central Europe: does the resolution matter?, Frontiers in Earth Science, 7, 290, https://doi.org/10.3389/feart.2019.00290, 2019.

Palacios-Peña, L., Fast, J. D., Pravia-Sarabia, E., and Jiménez-Guerrero, P.: Sensitivity of aerosol optical properties to the aerosol size distribution over central Europe and the Mediterranean Basin using the WRF-Chem v.3.9.1.1 coupled model, Geoscientific Model Development, 13, 5897–5915, https://doi.org/10.5194/gmd-13-5897-2020, 2020.

Parajuli, S. P., Stenchikov, G. L., Ukhov, A., and Kim, H.: Dust emission modeling using a new high-resolution dust source function in WRF-Chem with implications for air quality, Journal of Geophysical Research: Atmospheres, 124, 10 109–10 133, https://doi.org/10.1029/2019JD030248, 2019.

Pey, J., Querol, X., Alastuey, A., Forastiere, F., and Stafoggia, M.: African dust outbreaks over the Mediterranean Basin during 2001–2011: PM 10 concentrations, phenomenology and trends, and its relation with synoptic and mesoscale meteorology, Atmospheric Chemistry and Physics, 13, 1395–1410, https://doi.org/10.5194/acp-13-1395-2013, 2013.

Pino-Carmona, M., Ruiz-Arias, J. A., FernÃ¡ndez-Carvelo, S., Bravo-Aranda, J. A., and Alados-Arboledas, L.: Intercomparison of WRF-chem aerosol schemes during a dry Saharan dust outbreak in Southern Iberian Peninsula, Atmospheric Environment, 339, 120 872, https://doi.org/10.1016/j.atmosenv.2024.120872, 2024.

https://doi.org/10.5194/egusphere-2026-2127
Preprint. Discussion started: 22 April 2026

Poggio, L., de Sousa, L. M., Batjes, N. H., Heuvelink, G. B. M., Kempen, B., Ribeiro, E., and Rossiter, D.: SoilGrids 2.0: producing soil information for the globe with quantified spatial uncertainty, SOIL, 7, 217–240, https://doi.org/10.5194/soil-7-217-2021, 2021.

Querol, X., Pey, J., Pandolfi, M., Alastuey, A., Cusack, M., Pérez, N., Moreno, T., Viana, M., Mihalopoulos, N., Kallos, G., et al.: African dust contributions to mean ambient PM10 mass-levels across the Mediterranean Basin, Atmospheric Environment, 43, 4266–4277, https://doi.org/10.1016/j.atmosenv.2009.06.013, 2009.

Rahmati, O., Mohammadi, F., Ghiasi, S. S., Tiefenbacher, J., Moghaddam, D. D., Coulon, F., Nalivan, O. A., and Bui, D. T.: Identifying sources of dust aerosol using a new framework based on remote sensing and modelling., The Science of the total environment, 737, 139 508, https://doi.org/10.1016/j.scitotenv.2020.139508, 2020.

Ratcliffe, N. G., Ryder, C. L., Bellouin, N., Woodward, S., Jones, A., Johnson, B., Wieland, L.-M., Dollner, M., Gasteiger, J., and Weinzierl, B.: Long-range transport of coarse mineral dust: an evaluation of the Met Office Unified Model against aircraft observations, Atmospheric Chemistry and Physics, 24, 12 161–12 181, https://doi.org/10.5194/acp-24-12161-2024, 2024.

Regional SINQLAIR air quality network: https://sinqlair.carm.es/calidadaire/, Last access: 2026-01-23, 2018.

Rizza, U., Barnaba, F., Miglietta, M. M., Mangia, C., Di Liberto, L., Dionisi, D., Costabile, F., Grasso, F., and Gobbi, G. P.: WRF-Chem model simulations of a dust outbreak over the central Mediterranean and comparison with multi-sensor desert dust observations, Atmospheric Chemistry and Physics, 17, 93–115, https://doi.org/10.5194/acp-17-93-2017, 2017.

Salvador, P., Pey, J., Pérez, N., Querol, X., and Artíñano, B.: Increasing atmospheric dust transport towards the western Mediterranean over 1948–2020, npj Climate and Atmospheric Science, 5, 34, https://doi.org/10.1038/s41612-022-00256-4, 2022.

Schraufnagel, D. E.: The health effects of ultrafine particles, Experimental & molecular medicine, 52, 311–317, https://doi.org/10.1038/s12276-020-0403-3, 2020.

Segado-Moreno, L. C. and Montavez, J. P.: EROD Tuner, https://doi.org/10.5281/zenodo.18606994, 2026.

Segado-Moreno, L. C., Montavez, J. P., Raluy-López, E., Garnés-Morales, G., and Jiménez-Guerrero, P.: EROD-HR – A High Resolution Global Dust Erodibility Dataset , https://doi.org/10.5281/zenodo.18594482, 2026a.

Segado-Moreno, L. C., Montavez, J. P., Raluy-López, E., Garnés-Morales, G., and Jiménez-Guerrero, P.: SOILHD – Soil-Type Heterogeneous Erodibility Dataset , https://doi.org/10.5281/zenodo.18596292, 2026b.

Spyrou, C., Solomos, S., Bartsotas, N. S., Douvis, K. C., and Nickovic, S.: Development of a Dust Source Map for WRF-Chem Model Based on MODIS NDVI, Atmosphere, 13, https://doi.org/10.3390/atmos13060868, 2022.

Stewart, I. D. and Oke, T. R.: Local climate zones for urban temperature studies, Bulletin of the American Meteorological Society, 93, 1879–1900, https://doi.org/10.1175/BAMS-D-11-00019.1, 2012.

Tan, C., Liu, C., Li, T., Luan, Z., Tang, M., and Zhao, T.: A Dynamically Updated Dust Source Function for Dust Emission Scheme: Improving Dust Aerosol Simulation on an East Asian Dust Storm, Atmosphere, https://doi.org/10.3390/atmos16040357, 2025.

Tarín-Carrasco, P., Im, U., Geels, C., Palacios-Peña, L., and Jiménez-Guerrero, P.: Contribution of fine particulate matter to present and future premature mortality over Europe: A non-linear response, Environment International, 153, 106 517, https://doi.org/10.1016/j.envint.2021.106517, 2021.

Tegen, I. and Schepanski, K.: The global distribution of mineral dust, in: IOP Conference Series: Earth and Environmental Science, vol. 7, p. 012001, IOP Publishing, https://doi.org/10.1088/1755-1307/7/1/012001, 2009.

Tong, D. Q., Gill, T. E., Sprigg, W. A., Van Pelt, R. S., Baklanov, A. A., Barker, B. M., Bell, J. E., Castillo, J., Gassó, S., Gaston, C. J., et al.: Health and safety effects of airborne soil dust in the Americas and beyond, Reviews of Geophysics, 61, https://doi.org/10.1029/2021RG000763, 2023.

https://doi.org/10.5194/egusphere-2026-2127
Preprint. Discussion started: 22 April 2026

Ukhov, A., Ahmadov, R., Grell, G., and Stenchikov, G.: Improving dust simulations in WRF-Chem model v4. 1.3 coupled with GOCART aerosol module, Geoscientific Model Development Discussions, 2020, 1–30, https://doi.org/10.5194/gmd-14-473-2021, 2020.

Yarragunta, Y., Francis, D., Fonseca, R., and Nelli, N.: Evaluation of the WRF-Chem performance for the air pollutants over the United Arab Emirates, Atmospheric Chemistry and Physics, 25, 1685–1709, https://doi.org/10.5194/acp-25-1685-2025, 2025.

Zeng, Y., Wang, M., Zhao, C., Chen, S., Liu, Z., Huang, X., and Gao, Y.: WRF-Chem v3. 9 simulations of the East Asian dust storm in May 2017: modeling sensitivities to dust emission and dry deposition schemes, Geoscientific Model Development, 13, 2125–2147, https://doi.org/10.5194/gmd-13-2125-2020, 2020.

Zhao, A., Ryder, C., and Wilcox, L.: How well do the CMIP6 models simulate dust aerosols?, Atmospheric Chemistry and Physics, https://doi.org/10.5194/acp-2021-578, 2021.

Zhao, J., Ma, X., Wu, S., and Sha, T.: Dust emission and transport in Northwest China: WRF-Chem simulation and comparisons with multi-sensor observations, Atmospheric Research, 241, 104 978, https://doi.org/10.1016/j.atmosres.2020.104978, 2020.